

การพัฒนาวัสดุเชิงประกอบอะลูมินา-เซอร์โคเนียเพื่อใช้ทำลูกบิด



กมล ปานม่วง

สถาบันวิทยบริการ

จุฬาลงกรณ์มหาวิทยาลัย

วิทยานิพนธ์นี้เป็นส่วนหนึ่งของการศึกษาตามหลักสูตรปริญญาวิทยาศาสตรมหาบัณฑิต

สาขาวิชาเทคโนโลยีเซรามิก ภาควิชาวัสดุศาสตร์


คณะวิทยาศาสตร์ จุฬาลงกรณ์มหาวิทยาลัย

ปีการศึกษา 2546

ISBN 974-174-467-6

ลิขสิทธิ์ของจุฬาลงกรณ์มหาวิทยาลัย

DEVELOPMENT OF ALUMINA-ZIRCONIA COMPOSITE FOR MILLING BALL



Kamol Panmaung

สถาบันวิทยบริการ
จุฬาลงกรณ์มหาวิทยาลัย

A Thesis Submitted in Partial Fulfillment of the Requirements
for the Degree of Master of Science in Ceramic Technology

Department of Materials Science

Faculty of Science

Chulalongkorn University

Academic Year 2003

ISBN 974-174-467-6

Thesis Title Development of alumina-zirconia composite for milling ball
By Kamol Panmaung
Department Materials Science
Thesis Advisor Professor Shigetaka Wada (Ph.D.)
Thesis Co-advisor Associate Professor Supatra Jinawath (Ph.D.)

Accepted by the Faculty of Science, Chulalongkorn University in Partial
Fulfillment of the Requirements for the Master's Degree

.....Dean of Faculty of Science
(Professor Piamsak Menasveta, Ph.D.)

THESIS COMMITTEE

.....Chairman
(Associate professor Saowaroj Chuayjuljit)

.....Thesis Advisor
(Professor Shigetaka Wada, Ph.D.)

.....Thesis Co-advisor
(Associate Professor Supatra Jinawath, Ph.D.)

.....Member
(Associate Professor Paipan Suntisuk)

.....Member
(Sirithan Jiemsirilers, Ph.D.)

กมล ปานม่วง : การพัฒนาวัสดุเชิงประกอบอะลูมินา-เซอร์โคเนียเพื่อใช้ทำลูกบด.
(DEVELOPMENT OF ALUMINA-ZIRCONIA COMPOSITE FOR MILLING BALL) อ. ที่
ปริกษา : ศ.ดร. ชิกิตากะ วาดะ , อ.ที่ปริกษา ร่วม : รศ.ดร. สุพัตรา จินาวัฒน์ 62 หน้า. ISBN
974-174-467-6.

ในการทดลองนี้ ใช้ผงอลูมินา และผงเซอร์โคเนีย ทั้งที่มีโครงสร้างผลึกแบบ เตตระโกนอล และ โมโนคลินิก ในการพัฒนาวัสดุเชิงประกอบอลูมินา-เซอร์โคเนีย (3-9 % โดยน้ำหนัก) โดยทำการ บดผสมในหม้อบดแบบ แอตตรีชั่นเป็นเวลา 10 ชั่วโมง แล้วนำส่วนผสมไปขึ้นรูปเป็นเม็ดกลม แล้วเผา ซินเทอร์ที่อุณหภูมิตั้งแต่ 1500-1650°C ทำการวัดความหนาแน่น การเปลี่ยนแปลงของโครงสร้างผลึก สมบัติทางกายภาพ และ โครงสร้างจุลภาค ซึ่งผลการทดลองแสดงว่า เกรนของ เซอร์โคเนียไปยับยั้งการ โตของเนื้ออลูมินา ค่าVickers hardness และ fracture toughnessเพิ่ม ขึ้น เมื่อปริมาณของเซอร์โค เนียเพิ่มขึ้น โดยค่าVickers hardness และ fracture toughnessที่สูงสุดคือ 19.5GPa และ 3.05 MPam^{1/2} ตามลำดับ



สถาบันวิทยบริการ
จุฬาลงกรณ์มหาวิทยาลัย

ภาควิชาวัสดุศาสตร์
สาขาวิชาเทคโนโลยีเซรามิก
ปีการศึกษา 2003

ลายมือชื่อนิสิต.....
ลายมือชื่ออาจารย์ที่ปริกษา.....
ลายมือชื่ออาจารย์ที่ปริกษา ร่วม.....

4472203423 : MAJOR CERAMIC TECHNOLOGY

KEY WORD: ALUMINA / ZIRCONIA / COMPOSITE / HARDNESS / WEAR RESISTANCE

KAMOL PANMAUNG : THESIS TITLE. (DEVELOPMENT OF ALUMINA-ZIRCONIA COMPOSITE FOR MILLING BALL) THESIS ADVISOR : PROF. SHIGETAKA WADA (Ph.D.), THESIS COADVISOR : ASST.PROF. SUPATRA JINAWATH (Ph.D), 62 pp. ISBN 974-174-467-6.

In this study, alumina-zirconia (3-9 wt % ZrO₂) composites were produced from tetragonal (t-phase) and monoclinic (m-phase) zirconia and alumina powders. The formulated compositions were ground in an attrition mill for 10hr. Then they were each pressed into pellets and sintered in air atmosphere at temperatures ranging from 1500-1650°C. The relative density, phase transformation, mechanical properties and microstructures of the composites were investigated. The results show that zirconia grains inhibit grain growth of alumina matrix. Vickers hardness and fracture toughness increase with increasing of zirconia content and the maximum Vickers hardness and fracture toughness are 19.5GPa and 3.05 MPam^{1/2}, respectively.



Department..... Student's signature.....
Field of study..... Advisor's signature.....
Academic year 2003 Co-advisor's signature.....

Acknowledgements

I would like to express my gratefulness to my advisor, Professor Dr. Shigetaka Wada, for his guidance, encouragement and for all which I have learnt from him throughout this research. I would like to extend my gratitude to my co-advisor, Asst. Professor Dr. Supatra Jinawat, for giving me kind advice.

I would like to thank the National Metal and Materials Technology Center (MTEC) for the research grant, the Department of Chemical Engineering, Faculty of Engineering; the Department of Geology, the Department of Materials Science, Faculty of Science, and the Scientific and Technological Research Equipment Center, Chulalongkorn University, for providing the experimental facilities. Moreover, I would like to thank Chemmin Co., Ltd. for presenting us the AM-21 Al₂O₃ powder.

Finally, I would like to gratitude to my family for their loves, understanding and encouragement.



สถาบันวิทยบริการ
จุฬาลงกรณ์มหาวิทยาลัย

CONTENTS

Page

Abstract (Thai).....	iv
Abstract (English).....	v
Acknowledgements.....	vi
Contents.....	vii
List of Tables.....	ix
List of Figures.....	x
Chapter 1 Introduction.....	1
Chapter 2 Literature review.....	3
2.1) Sintering of alumina.....	3
2.2) Effect of additive.....	5
2.2.1) Effect of MgO.....	5
2.2.2) Effect of ZrO ₂	7
2.2.3) Transformation toughening.....	8
Chapter 3 Experimental procedure.....	10
3.1) Raw materials and characterization.....	10
3.1.1) Raw materials.....	10
3.1.2) Characterization of raw materials.....	11
3.1.2.1) Particle Size Distribution.....	11
3.1.2.2) X-Ray Diffraction.....	11
3.2) Composition and powder preparation.....	11
3.3) Characterization of sintered specimens.....	14
3.3.1) Density.....	14
3.3.1.1) Bulk density.....	14
3.3.1.2) Water absorption.....	14
3.3.1.3) Theoretical density.....	14
3.3.1.4) Relative density.....	14

CONTENTS (Cont.)

Page

3.3.2) Microstructure investigation by SEM.....	16
3.3.3) Mechanical properties.....	16
3.3.3.1) Vickers hardness.....	16
3.3.3.2) Fracture toughness.....	17
Chapter 4 Experimental results and discussions.....	18
4.1) Characterization of raw materials.....	18
4.1.1) Particle Size Distribution.....	18
4.1.2) X-Ray Diffraction.....	19
4.2) Densities of sintered specimens.....	21
4.3) Mechanical properties.....	22
4.3.1) Vickers hardness.....	22
4.3.2) Fracture toughness.....	23
4.4) Microstructure.....	25
4.5) XRD results of the sintered specimens.....	28
Chapter 5 Conclusions.....	29
Chapter 6 Future works.....	30
References.....	31
Appendices.....	33
1. Particle size distribution.....	34
2. Density.....	39
3. Vickers hardness and fracture toughness.....	43
4. SEM micrographs.....	45
5. Average grain size.....	51
6. X – ray diffraction profiles.....	55

LIST OF TABLES

	Page
Table 3.1 Oxide powders and chemicals used in this experiment.....	10
Table 3.2 Compositions of Alumina powders in this experiment.....	12
Table 3.3 Calculated theoretical density of each composition.....	15
Biography.....	63



สถาบันวิทยบริการ
จุฬาลงกรณ์มหาวิทยาลัย

LIST OF FIGURES

Page

Fig 2.1 Schematic of the geometry of sintering of two spheres, showing six.....3 Alternate paths for matter transport	
Fig 2.2 Effect of MgO content on the density of sintered alumina.....5	
Fig 2.3 Schematic of the toughening mechanism in alumina-zirconia ceramic.....8	
Fig 2.4 Flexure strength and toughness of alumina as a function of zirconia addition.....9	
Fig 3.1 Flow diagram of sample preparation using Attrition mill.....13	
Fig 4.1 Average particle size distribution of AM-21 alumina powder crushed.....18 for 10 hours	
Fig 4.2 Average particle size distribution of SPZ zirconia powder crushed.....19 for 10 hours	
Fig 4.3 XRD patterns of as-received ZrO ₂ powders (monoclinic SPZ and.....20 tetragonal GTYS-5 powders)	
Fig 4.4 Relationships between densities and sintering temperatures of KM01-08.....21	
Fig 4.5 Vickers hardness of specimens sintered at 1600°C22	
Fig 4.6 Vickers hardness of specimens sintered at 1650°C23	
Fig 4.7 Fracture toughness of specimens sintered at 1600°C24	
Fig 4.8 Fracture toughness of specimens sintered at 1650°C24	
Fig 4.9 Relationships between average grain size and ZrO ₂ content.....25	
Fig 4.10 (a) SEM micrograph of 6% SPZ added specimen, sintered at 1600°C.....26 (b) SEM micrograph of 6% GTYS-5 added specimen, sintered at 1600°C.....26	
Fig 4.11 (a) SEM micrograph of 6% SPZ added specimen, sintered at 1650°C.....27 (b) SEM micrograph of 6% GTYS-5 added specimen, sintered at 1650°C.....27	
Fig 4.12 XRD patterns of sintered specimens (in pellets) of KM05 at 1600.....28 and 1650°C	

Chapter 1

Introduction

Theory:

Erosive wear⁽¹⁻⁴⁾ and wear of media during milling⁽⁵⁾ are strongly dependent on the hardness ratio H_p/H_m , here H_p is the hardness of particle which will be crushed and H_m is the hardness of media ball. When $H_p/H_m < 1$, wear of balls is small. Fracture toughness of media balls also affects the wear of balls during milling. When the fracture toughness (K_{IC}) of media is high, wear of media is low. Typical method for improving the K_{IC} of a ceramic is to make a composite. Considering the cost of production, the most popular material for media ball is alumina (Al_2O_3)-zirconia (ZrO_2) composite.

Usually, high purity alumina ceramics are produced from fine alumina powder with high purity, such as AKP of Sumitomo and Timicron. However, the price of these powders are so expensive (2,000-3,000 B/kg). When cheap alumina powder is used, it is difficult to sinter ceramics to full density at some not too high temperature as 1650°C. With the addition of sintering aids, i.e. SiO_2 , MgO and etc., the hardness of the alumina ceramics decreases. Recently, Dr. S. Sirisunthorn had developed a technology to sinter alumina ceramics at about 1600-1650°C using low price Al_2O_3 powder AM-21 without sintering additives. In his experiment, AM-21 (36 B/kg, Sumitomo Chemicals, Japan) was crushed using zirconia (ZrO_2) balls. In this case, zirconia does not work as sintering aid but works as grain growth inhibitor. Although zirconia ball is not the best material for crushing alumina because it is expensive (>5,000 B/kg) and wears easily, the composite between Al_2O_3 - ZrO_2 has been known to have a rather large K_{IC} ⁽⁶⁾. The hardness of Al_2O_3 - ZrO_2 composite decreases with increasing content of ZrO_2 . However, the decrease in hardness is not significant when the content of ZrO_2 is less than 5 wt%. From our previous experiments, it was found that ZrO_2 less than 5 wt% could disturb the grain growth of alumina ceramic. The hardness of alumina ceramics is about 15-20 GPa, and that of zirconia is about 12-13 GPa, hence alumina ceramics are more wear resistant than zirconia ceramics. As mentioned, zirconia ball is very expensive because of the high cost of zirconia powders, for example, TOSO TZY which is the most popular one in the world, is about 3,000 B/kg. However, DAIICHI-KIGENSO's SPZ and FUKUSHIMA

SEIKO's GTYS-5 are cheaper, about 1,000 B/kg. Considering from all the fact mentioned, crushing low price Al_2O_3 powder with small amount of low price ZrO_2 as additive, using Al_2O_3 balls, will be the most practical process to get a composite powder that can be sintered at moderate temperatures.

Objectives:

The objective of this project is to establish a condition to get excellent wear resistant Al_2O_3 based material for media balls which is better in quality but cheaper in cost than NIKKATO SSA-995 and HD grade, using very cheap raw Al_2O_3 powder. The immediate goal is to get a ceramic consisting of Al_2O_3 - ZrO_2 composite with Vickers hardness of >17 GPa (at 10 kg) and fracture toughness of $>5-6$ $\text{MPam}^{1/2}$ (about twice that of pure alumina). The final goal of this research is to develop an excellent Al_2O_3 based media balls for ceramic industries. In pursuing the final goal after achieving the immediate one, the project on developing an appropriate technology for forming media balls and evaluation of the wear resistance will be proposed as future work.



สถาบันวิทยบริการ
จุฬาลงกรณ์มหาวิทยาลัย

Chapter 2

Literature review

2.1 Sintering of alumina

The sintering phenomena of materials are classified into 3 stages that are initial, intermediate and final stages, respectively.

The sintering phenomena in material consist of the dominant mechanism by which matter transport occurs⁽⁷⁾. The sintering phenomena of Al_2O_3 are solid state sintering. The driving force of sintering in the solid state has early been recognized to be the surface tension. The kinetics of the process, however; may be controlled during the initial stage of sintering by diffusion processes, which defines different paths for matter transport.

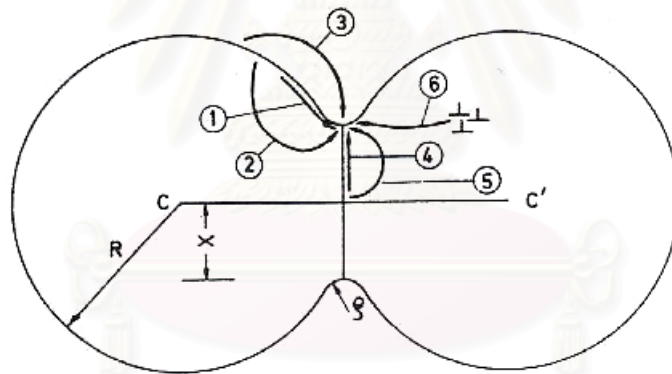


Fig.2.1 Schematic of the geometry of sintering of two spheres, showing six alternate paths for matter transport⁽⁸⁾.

Fig 2.1 shows the typical sintering geometry between two powder particles according to Kingery and Berg⁽⁸⁾. According to Ashby⁽⁹⁾, there are six paths for matter transport as following

- (1) surface diffusion,
- (2) lattice diffusion from the surface region,
- (3) vapor transport,

- (4) boundary diffusion,
- (5) lattice diffusion from boundary region, and
- (6) lattice diffusion from dislocations or other internal sources to the neck surface.

The growth of the neck on the initial sintering of alumina is formed between a sphere and a plate as a function of time and sphere radius. The shrinkage of powder compacts is a function of time at various temperatures ⁽¹⁰⁾. The initial stage is characterized by the neck growth between the original powder particles and a slight increase in density of about 10%. The kinetics and size dependence of the sintering of alumina follow the sintering model ⁽⁸⁾. This model is based on the assumptions that the driving force for solid state sintering is the surface tension, the dominant transport mechanism is lattice diffusion, and the grain boundaries operate as vacancy sinks. The later stages of sintering are decisive for the final density of the product. The beginning of the immediate stage coincides with the beginning of grain growth. During this stage, particles grow to a grain-like structure, the pore phase forming an array for interconnected cylindrical channels lying on three-grain edges. The final stage starts at about 95% porosity, when cylindrical pores are transformed into spherical voids by a pinch-off process. The pore phase is now present as discontinuous pores lying at four-grain corner ⁽¹¹⁾.

During sintering of intermediate and final-stage sintering kinetics in alumina, the porosity decreases linearly with the logarithm of time. The necessary condition to achieve theoretical density in solid stage sintering consists of eliminating or suppressing the occurrence of discontinuous grain growth ⁽⁷⁾. Grain boundaries will remain attached to the pores and the normal grain growth will be sufficiently slow that the pores can move off the grain boundaries and do not become trapped inside the grains. Since the pore phase remains intersected by the boundaries, the diffusion path is short and facilitates the complete removal of porosity.

2.2 Influence of additives

Alumina can be sintered to achieve theoretical density⁽¹²⁾ and it has been known that additives may have a beneficial influence on the sintering kinetic of alumina.

2.3.1 Effect of MgO

Magnesium oxide is the most widely used additive in the sintering of alumina. Adding small amount of MgO will prevent discontinuous grain growth and allow the material to be sintered to theoretical or nearly theoretical density⁽¹²⁾. Discontinuous grain growth means that grain boundaries break away from the pores, thereby including the pores inside the new large grains^(12,13).

Several experimental studies demonstrate that alumina may be sintered to theoretical density using MgO additions even below the solubility limit.

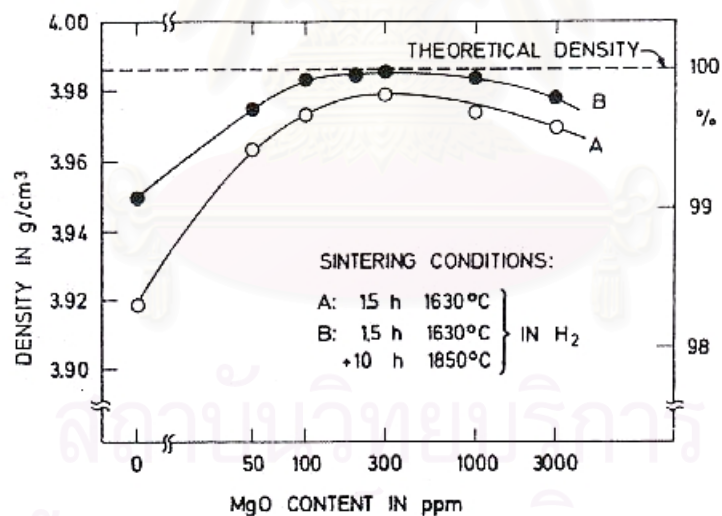


Fig.2.2 Effect of MgO content on the density of sintered alumina.

Fig 2.2 shows the density results from the work of Peelen⁽¹⁴⁾, who sintered specimens containing between 0 and 3000 ppm MgO. A maximum density was found at 300 ppm MgO, which was just the solubility limit reported⁽¹⁵⁾ at the sintering temperature of 1630 °C. This result is evidence that the densification rate in the absence of discontinuous grain growth is controlled by the solute concentration.

The beneficial effect of the MgO additive is due to the increase of the densification rate (pore removal rate) with respect to the grain growth rate. In the other words, the ratio of the pore mobility to the grain boundary mobility, M_p/M_b , must exceed a certain value. An increase in the pore mobility will favor the increase of the mobility ratio^(16,17).

In the case of pore movement due to surface diffusion, the pore mobility is given by the expression⁽¹⁸⁾.

$$M_p = KD_s/r^4 \quad (2.1)$$

Where D_s is the surface diffusion coefficient,
 r is the pore radius, and
 K is a constant.

The sintered product of MgO-doped alumina sample will have a smaller pore size compared to a sample made of pure alumina because the presence of the dopant increases the rate of pore removal. Therefore, the doped material will also be characterized by a greater pore mobility which is simply due to the size effect given by equation (2.1), and hence will show a decrease or retard tendency for discontinuous grain growth⁽¹⁷⁾.

สถาบันวิทยบริการ
จุฬาลงกรณ์มหาวิทยาลัย

2.3.2 Effect of ZrO₂

Grain growth inhibition is desirable for preventing abnormal grain growth during sintering, which allows pores to be swallowed to limit end-point densities, and for limiting grain size to achieve higher strengths. Second-phase inclusions can inhibit grain growth. Theory that treats the inhibition of grain growth by inclusion has generally been on refinements of Zener's original concept⁽¹⁹⁾, in which the inclusion residing at the grain boundary produces a dragging force due to the lower free energy of the junction/inclusion system when the inclusion resides at the junction. Ashby and Centamore⁽¹⁹⁾ showed that the inclusion could move with the junction if the inclusion exhibited sufficient self-diffusion. Theory suggests that the velocity of the moving inclusion will depend on its radius r as either r^{-3} or r^{-4} , for interfacial diffusion or volume diffusion, respectively.

Lange and Hirlinger⁽¹⁹⁾ reported that the materials containing ≤ 2.5 vol.% ZrO₂ were strongly bimodal at temperature ≥ 1600 °C, whereas grain growth control (normal grain growth) was achieved for ZrO₂ contents ≥ 5 vol.%. Microstructure of composites exhibited controlled grain growth (≥ 5 vol.% ZrO₂). Fracture surface observations showed that the ZrO₂ grains were primarily located at 4-grain junctions.

Abnormal grain growth occurred when the inclusion distribution was not sufficiently uniform to hinder the growth of all Al₂O₃ grains. This condition was observed for compositions containing ≤ 2.5 vol.% ZrO₂, where the inclusions did not fill all 4-grain junctions. Grain growth control (no abnormal grain growth) was achieved when a majority (or all) 4-grain junctions contained a ZrO₂ inclusion, viz., for compositions containing ≥ 5 vol.% ZrO₂. For this condition, the grain size was inversely proportional to the volume fraction of the inclusions.

2.2.3 Transformation toughening

The transformation of the tetragonal (t) to monoclinic (m) zirconia has been widely used to increase the toughness of ceramic materials, therefore a variety of ceramics have been employed as the ceramics matrix including cubic zirconia, alumina, mullite, silicon carbide, yttrium oxide, silicon nitride and so forth.

Pure ceramics have a fracture toughness between 0.2 and $2 \text{ MPam}^{1/2}$. However, a dispersion of particles of a second phase can increase this a little. Normally, the tetragonal material would transform to the monoclinic form during cooling, but it must expand to do so (about 3-5%)⁽²¹⁾. The high strength of the surrounding cubic zirconia prevent this expansion, so the tetragonal form is retained in a metastable tetragonal phase all the way down to room temperature⁽²²⁾. As a result, each tetragonal zirconia precipitate is under stress and full of energy that wants to be released. If a crack tries to break the ceramic, tetragonal precipitates next to the crack are now able to expand and transform back to their stable monoclinic form with a compressive strain being generated in the matrix. This expansion adjacent to the crack presses against the crack and both strength and toughness are increased significantly⁽²⁰⁾.

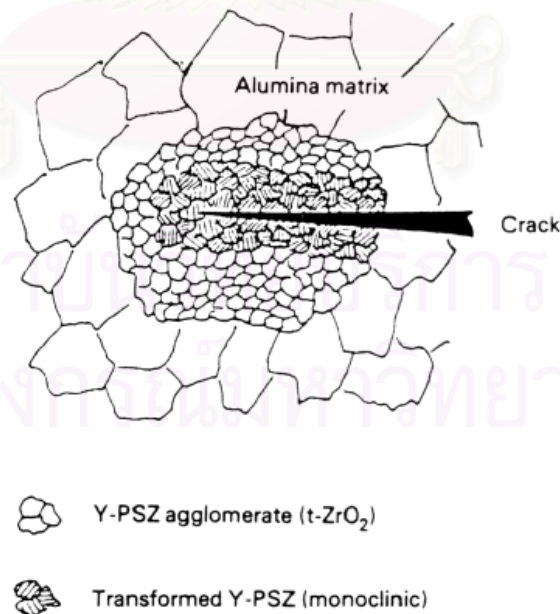


Fig.2.3 Schematic of the toughening mechanism in alumina-zirconia ceramic.

After sintering, a critical particle size range for zirconia exists. If the particles are less than a critical size on cooling down they will not transform; if they are larger than a critical size they will transform from tetragonal to monoclinic spontaneously. This critical size depends on the matrix constraint and the composition of the zirconia; as the cubic stabilizing oxide content is increased, the chemical free energy associated with the phase transformation decreased and hence larger particles can be induced to remain the metastable tetragonal form ⁽²¹⁾.

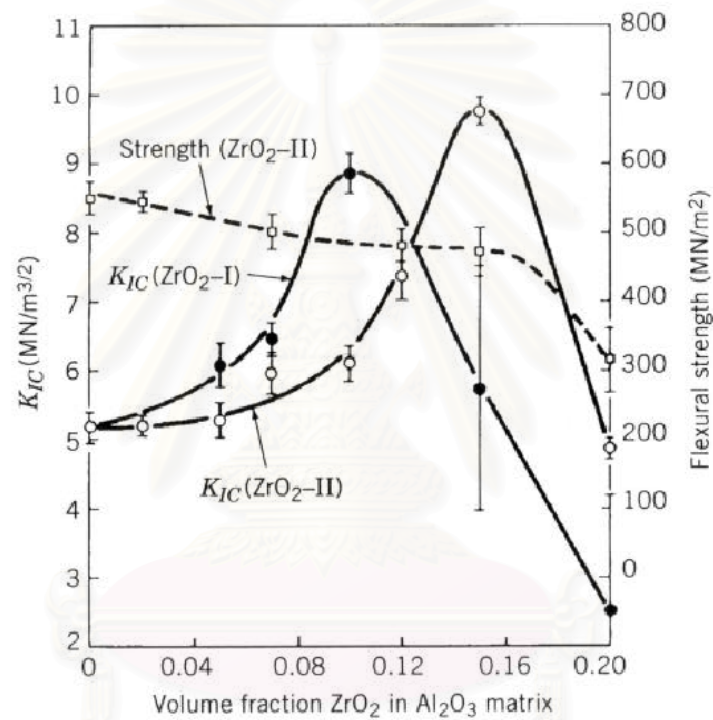


Fig.2.4 Flexure strength and toughness of alumina as a function of zirconia addition : I and II refer to 0.3 and 1.25 μ m zirconia particles.

Chapter 3

Experimental procedure

The experimental conditions, techniques of sample preparation and the measurements of physical and thermal properties as well as microstructure investigation are described in this chapter.

3.1 Raw materials and characterization

3.1.1 Raw materials

Oxides listed in Table 3.1 were used as starting raw materials. The composition data for each material was received from the suppliers.

Table. 3.1 Oxide powders and chemicals used in this experiment

Materials	Purity (%)	Average particle size(μm)	Manufacturers
Aluminium oxide AM-21	99.7	4	Sumitomo
Magnesium oxide			
Zirconium oxide SPZ	99.5	2	Daiichi-Kigenso
Zirconium oxide GTYS - 5	$\text{ZrO}_2 + \text{HfO}_2 : 93.71$	2	Fukushima

Aluminum oxide, AM-21 powder, was used as starting material considering from its purity and particle size shown in Table 3.1, and their cost; price of AM-21 is about 36 baht/Kg. SPZ and GTYS – 5 powders have crystal structures of monoclinic and tetragonal, respectively.

3.1.2 Characterization of raw materials

3.1.2.1 Particle size distribution determination

Particle size distribution of AM-21, SPZ and GTYS - 5 were measured using sedimentation centrifugal particle size analyzer (Shimadzu SA-CP2). About 1 gram of powder was mixed with 0.2 wt% NaHMP solution before subjected into the centrifugal particle size analyzer. A solution with 0.2wt% NaHMP was used as a blank solution.

3.1.2.2 X-Ray diffraction

Starting raw materials were investigated by XRD technique to specify crystal structure.

3.2 Composition and powder preparation

All compositions shown in Table 3.2 were prepared using attrition mills. The flow chart of preparation is illustrated in Fig 3.1. The raw materials were mixed with various additives, MgO and ZrO₂. Both additives prevent exaggerated grain growth and allow the material to be sintered to theoretical or nearly theoretical density. The amount of MgO was selected as 0.1 wt%. The amounts of ZrO₂ were selected as 3, 6 and 9 wt%. About 260 gram of the mixed powders were ground in an attrition mill for 10 hours, using alumina balls as grinding media and 180 ml of distilled water as solvent. Alumina balls were filled to a half volume of the milling pot. The slurry was sieved filtrated and dried at 105°C overnight in an oven to remove the water. Before forming, the obtained powder was well mixed with 1.0 wt% of polyvinyl alcohol (PVA with 9,000 – 10,000 MW (twenty grams 100 ml of water)) acted as a binder and was sieved through a 100 mesh sieve. The granules were pressed into pellets of 25 mm in diameter x 2 mm thickness by uniaxial hydraulic press with 18 MPa pressure. All specimens were heated to 500°C for 2 hours with heating rate of 5°C /min for binder removal then the temperature was raised at a heating rate of 5°C /min to 1,500, 1,550, 1,600 and 1,650°C with a soaking period of 2 hours for densification. The sintered samples were cooled to 35°C in the furnace.

Table.3.2 Compositions of Alumina powders in this experiment

Composition	Alumina	Additives (wt%)
KM01	AM-21	-
KM02	AM-21	0.1% MgO
KM03	AM-21	3% SPZ ZrO ₂
KM04	AM-21	6% SPZ ZrO ₂
KM05	AM-21	9% SPZ ZrO ₂
KM06	AM-21	3% GTYS-5 ZrO ₂
KM07	AM-21	6% GTYS-5 ZrO ₂
KM08	AM-21	9% GTYS-5 ZrO ₂



สถาบันวิทยบริการ
จุฬาลงกรณ์มหาวิทยาลัย

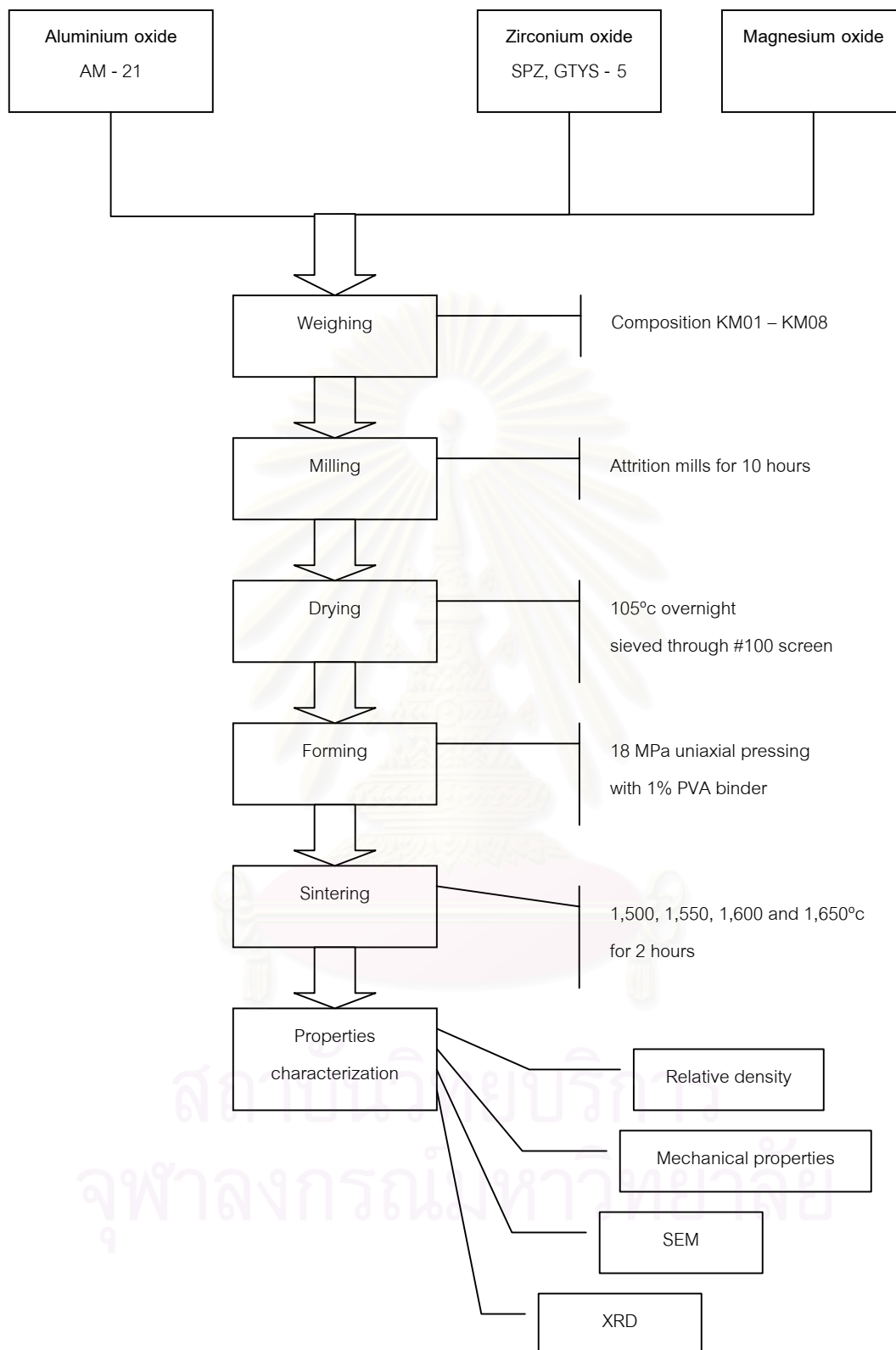


Fig. 3.1 Flow diagram of sample preparation using Attrition mill

3.3 Characterization of sintered specimens

3.3.1 Density

3.3.1.1 Bulk density

The bulk density of specimens was measured according to Archimedes' method. The air in open pores of specimen was removed by applying vacuum for 30 min and then water was poured onto specimens until submerged in water. Water was further forced into the opened pores by applying vacuum for 1 hr. The dry weight W_d , saturated weight W_{sat} and suspended weight W_{sus} were measured and used to calculate the bulk density using equation (3.1) following ASTM standard (Designation : C830-93).

$$\text{Bulk density} = \frac{W_d}{W_{sat} - W_{sus}} \rho \quad (3.1)$$

Where ρ is water density at the measurement temperature (0.99568 g/cm³ at 30 °C).

3.3.1.2 Water absorption

Water absorption of specimen was calculated according to equation (3.2)

$$\text{Water absorption (\%)} = \frac{W_{sat} - W_d}{W_d} \cdot 100 \quad (3.2)$$

Where W_{sat} is saturated weight and W_d is dry weight of the specimen.

3.3.1.3 Theoretical density

The theoretical density of sintered pellets was calculated from real density using the following equation:

$$\text{Theoretical density} = \frac{W_{\text{total}}}{W_a/\rho_a + W_b/\rho_b + \dots} \quad (3.3)$$

Where W_{total} is total weight of used components.

W_a, W_b are weights of component, a and b, respectively.

ρ_a, ρ_b are real densities of component, a and b, respectively.

a, b,... are used components.

In this experiment, the theoretical densities of pure $\text{Al}_2\text{O}_3 = 3.97 \text{ g/cm}^3$, $\text{MgO} = 3.64 \text{ g/cm}^3$ and $\text{ZrO}_2 = 6.023 \text{ g/cm}^3$ were used for calculation. As a result, theoretical density of compositions are calculated and shown in Table 3.3.

Table 3.3 Calculated theoretical density of each composition

Compositions	Calculated 100% density (g/cm^3)
KM01	3.97
KM02	3.97
KM03	4.01
KM04	4.05
KM05	4.09
KM06	4.01
KM07	4.05
KM08	4.09

3.3.1.4 Relative density

The relative density of the sintered specimens was calculated from its bulk density and theoretical density using the following equation:

$$\text{Relative density} = \frac{\text{Bulk density}}{\text{Theoretical density}} \quad (3.4)$$

and % of theoretical density = Relative density x 100.

3.3.2 Microstructure investigation by scanning electron microscope (SEM)

Microstructures of specimens sintered at 1,600°C and 1,650°C were examined using a scanning electron microscope (SEM) (JEOL : JSM-1670). The sintered specimens were polished with various sizes of silicon carbide powder, then thermally etched at 1,500°C for 30 min. The specimens were gold sputtered before subjected into the SEM investigation. The average grain size was determined by a line intercept method following ASTM standard (designation : E112 - 96).

3.3.3 Hardness and fracture toughness measurement

The compositions in Table 3.2 were pressed into pellets of 25 mm diameter by a hydraulic press with 18 MPa pressure. All specimens were sintered at 1,500, 1,550, 1,600 and 1,650°C for 2 hours. The surfaces of sintered samples were ground with silicon carbide powder to parallel surfaces.

3.3.3.1 Vickers hardness

Vickers hardness of sintered specimens was measured by Vickers hardness indentation machine. The specimens were polished by silicon carbide powder number 2,000 and 8,000, respectively and finished with diamond (6, 3 and 1µm powder, respectively) to get flat and glossy surface. Indentation load was 98 N. Vickers hardness was calculated from the following equation:

$$HV = 0.1891 F/d^2 \quad (3.5)$$

HV : Vickers hardness

F : test load (N)

d : average length of diagonal lines of dent (mm)

3.3.3.2 Fracture toughness

Fracture toughness was measured by the same indent as Vickers hardness. Fracture toughness was calculated from the following equation:

$$K_{IC} = 0.018(E/HV)^{1/2} (P/C^{3/2}) \quad (3.6)$$

K_{IC} : fracture toughness value ($\text{Pa m}^{1/2}$)

E : modulus of elasticity (Pa)

HV : Vickers hardness (GPa)

P : pressing-in load (N)

C : half of average of crack length (m)



สถาบันวิทยบริการ
จุฬาลงกรณ์มหาวิทยาลัย

Chapter 4

Results and discussions

4.1) Characterization of raw materials

4.1.1) Particle size distribution

AM-21 was crushed in attrition mill using balls of different sizes 5, 3 and 1 mm in average, respectively. The average sizes of AM-21 after 3 hr crushing were 0.8, 0.3 and 0.5 μm , respectively. Therefore, 3 mm ball was selected as media ball from now on. Particle size distribution curves are shown in Appendix 1.

All raw powders were crushed for 10 hours using attrition mills for particle size observation. The average particle sizes of all crushed powders are shown in Fig. 4.1 and 4.2.

The average particle sizes of all crushed powder are in the range of 0.2-0.4 μm after crushing for 10 hours. However, beyond 7 hours of crushing, there are very small difference of particle size distributions for both zirconia powders.

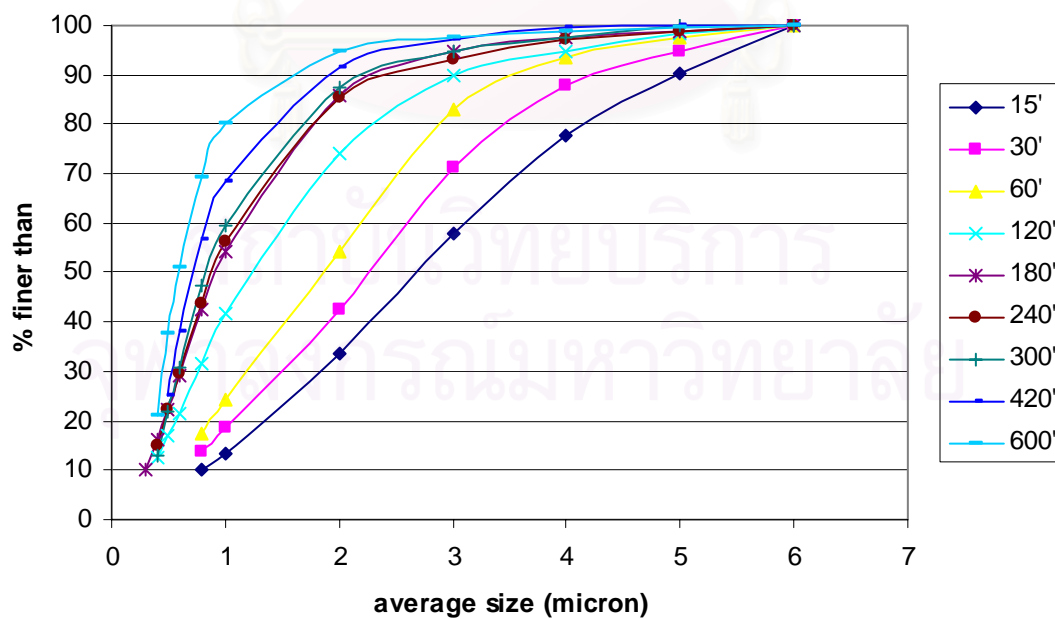


Fig 4.1 Average particle size distribution of AM-21 alumina powder crushed for 10 hours

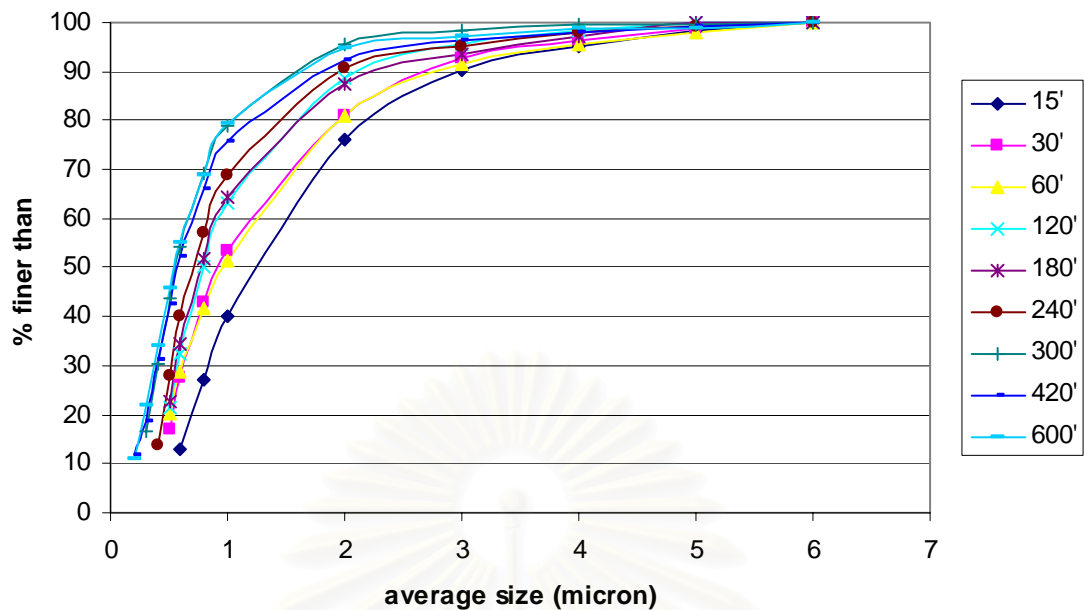


Fig 4.2 Average particle size distribution of SPZ zirconia powder crushed for 10 hours

4.1.2) X-Ray Diffraction

The x-ray diffraction patterns of raw powders are shown in Appendix 6. The XRD pattern of AM-21 alumina shows crystal structure of α - Al_2O_3 . While both SPZ and GTYS-5 zirconia powders show structures of monoclinic and tetragonal, respectively, as shown in Fig 4.3. SPZ ZrO_2 powder is identified as mainly monoclinic. Since SPZ does not include any dopants, it is reasonable to be monoclinic. GTYS-5 should be tetragonal because it includes 3 mol% Y_2O_3 . However, upon grinding the GTYS-5 ZrO_2 into powder, tetragonal to monoclinic transformation of ZrO_2 can occur, hence GTYS-5 powder shown is composed of a mixture containing tetragonal crystals as main phase and monoclinic crystals as minor phase.

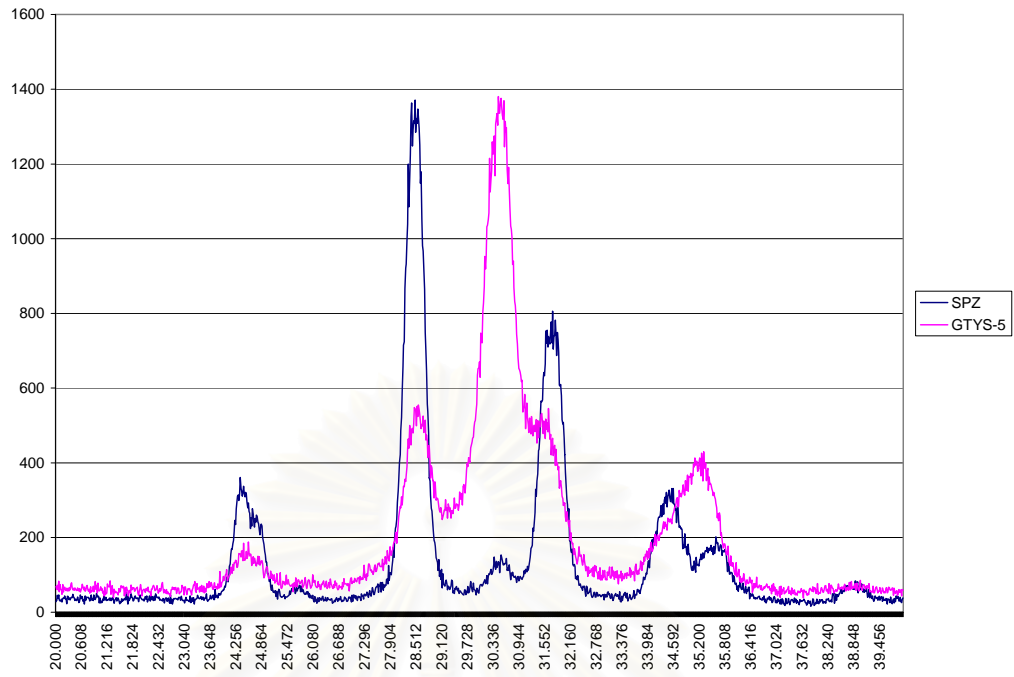


Fig.4.3 XRD patterns of as-received ZrO₂ additives (monoclinic SPZ and tetragonal GTYS-5 powders)

4.2) Densities of sintered specimens

Bulk gravity, water absorption and % of theoretical density are shown in appendix 2. Relationships between density and sintering temperatures of all specimens are also shown in Appendix 2.

The relationship between density and sintering temperatures is shown in Fig 4.4. Density reaches almost full density at 1600-1650°C. The compositions contain SPZ show higher density than those contain GTYS-5.

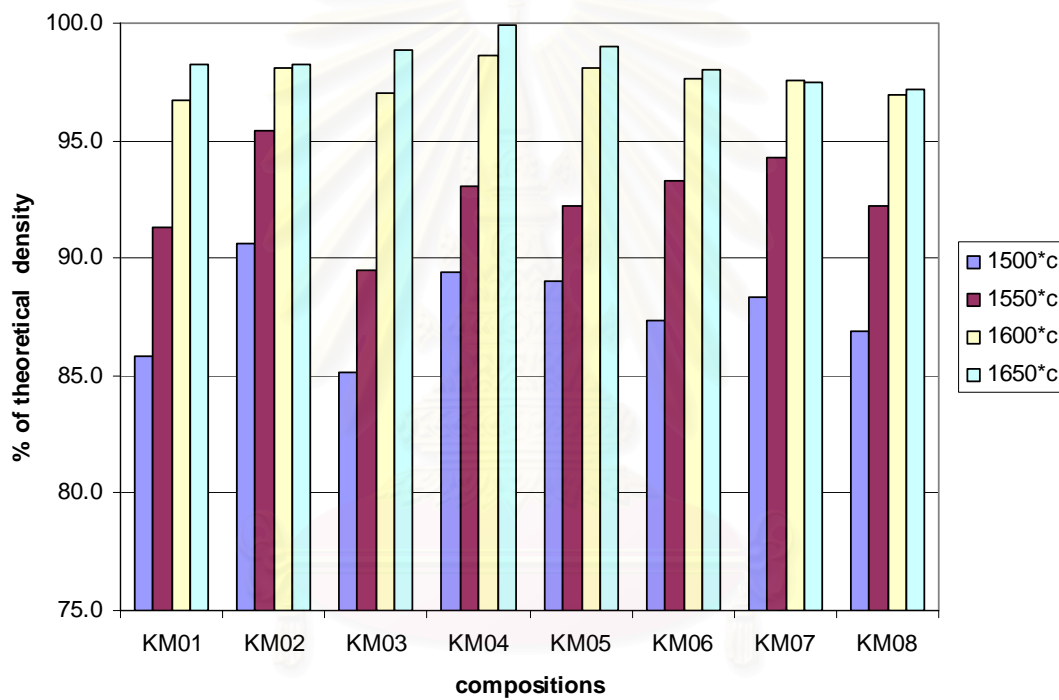


Fig 4.4 Relationships between density and sintering temperatures of KM01-08

4.3) Mechanical properties

4.3.1) Vickers hardness

Vickers hardness of all specimens sintered at 1600-1650°C are shown in Appendix 3. Vickers hardness of each composition is shown in Fig. 4.5 and 4.6. Specimens sintered at 1600°C have higher Vickers hardness than those sintered at 1650°C. 9% GTYS-5 added composition sintered at 1600°C shows the highest value of Vickers hardness.

Since the hardness of pure Al_2O_3 is about 20 GPa and that of pure ZrO_2 is about 12 GPa. Therefore, it is supposed that the composition with much amount of ZrO_2 , KM05 and KM08, will show low hardness. However, experimental results are reverse. It was said that smaller particle size specimens show larger hardness than large particle size specimens. Hence it is concluded that the particle size effect on hardness appears strongly in this experiment.

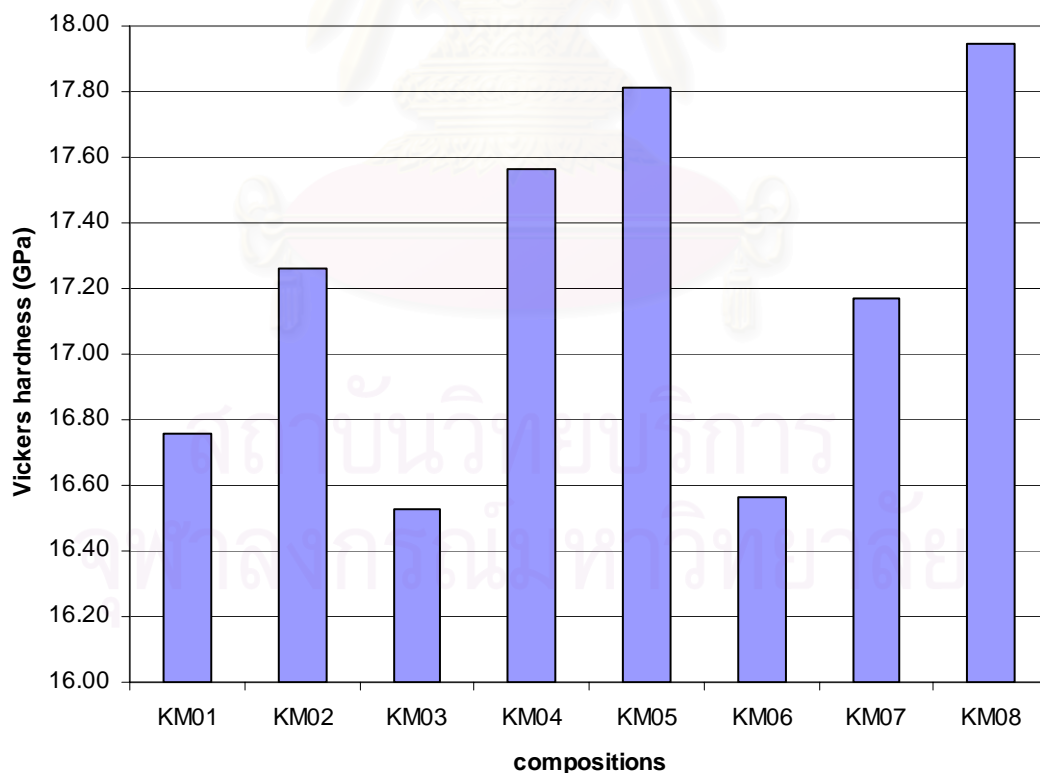


Fig. 4.5 Vickers hardness of specimens sintered at 1600°C

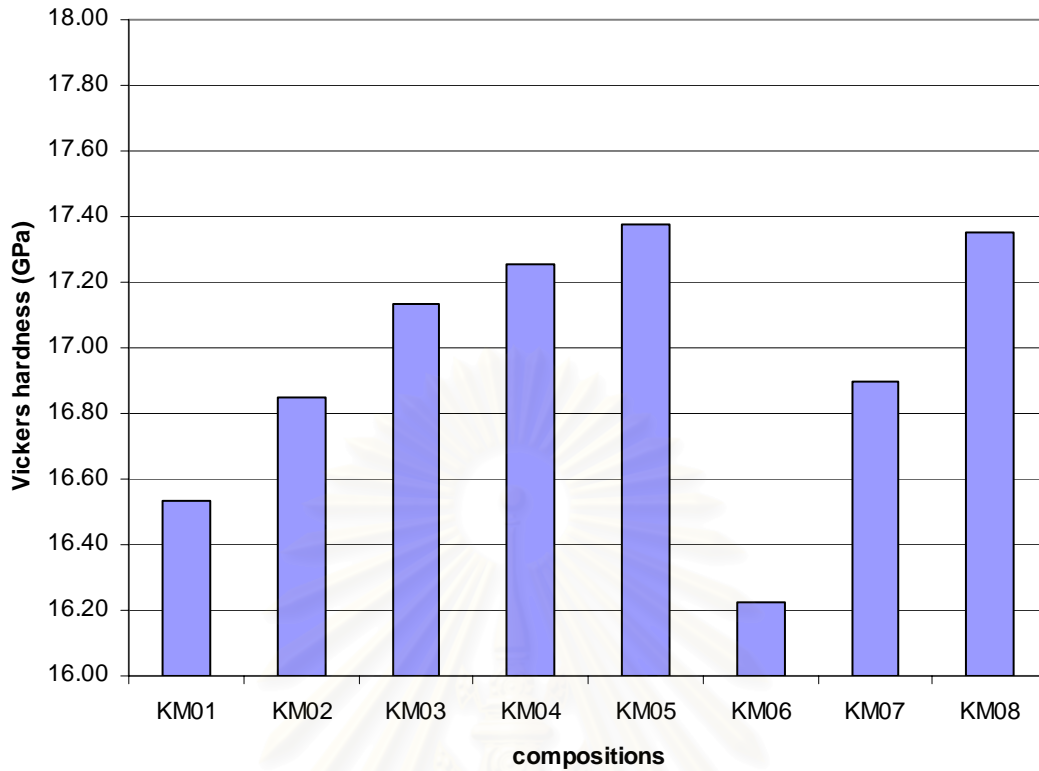


Fig.4.6 Vickers hardness of specimens sintered at 1650°C

4.3.2) Fracture toughness

Fracture toughness values of all specimens sintered at 1600-1650°C are shown in Appendix 3. Fracture toughness of each composition is shown in Fig 4.7 and 4.8. Specimens sintered at 1650°C have higher fracture toughness than those sintered at 1600°C in average. The composition containing 6% GTYS-5 shows the highest fracture toughness.

สถาบันวิทยบริการ
จุฬาลงกรณ์มหาวิทยาลัย

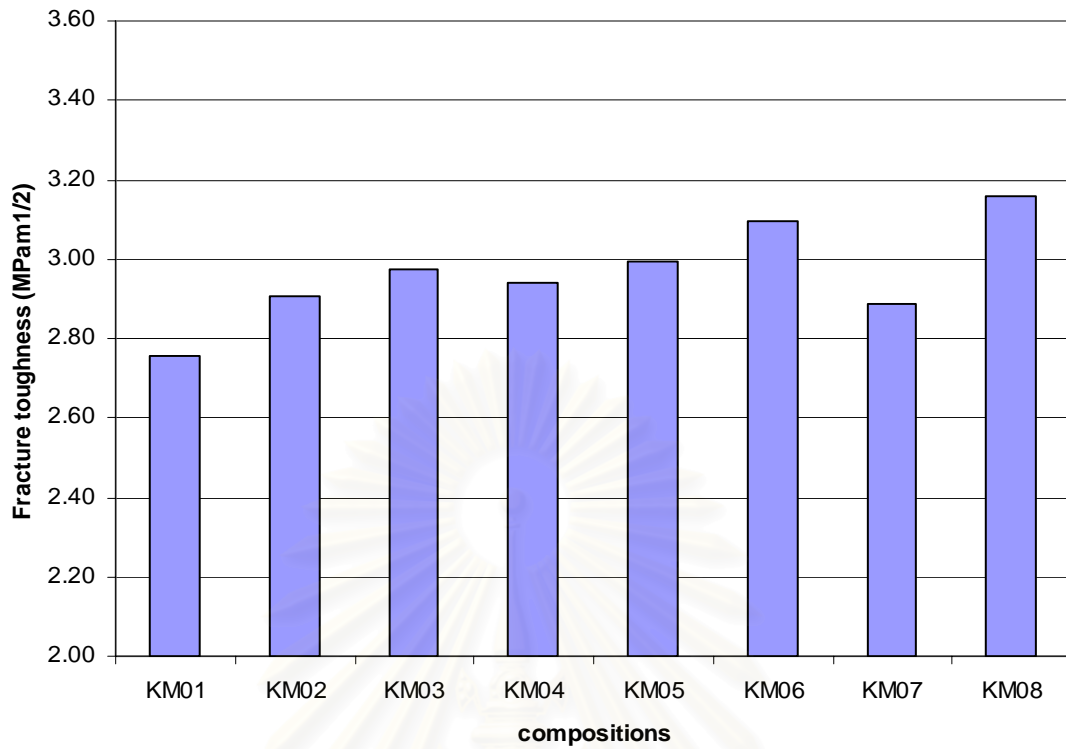


Fig.4.7 Fracture toughness of specimens sintered at 1600°C

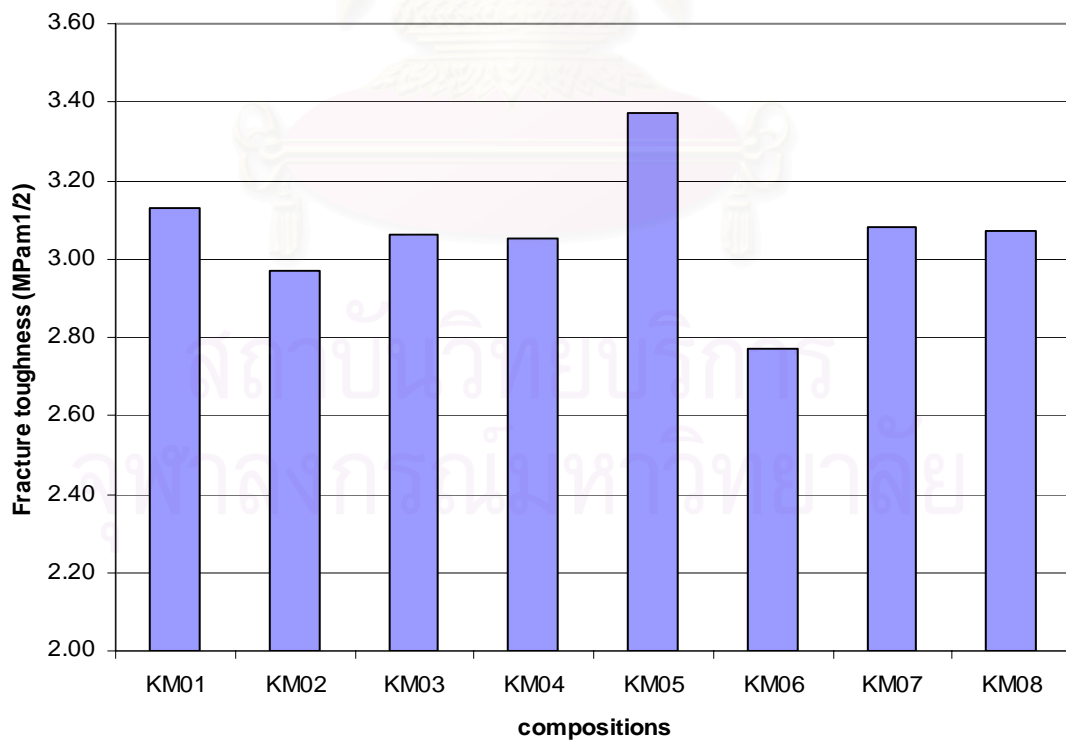


Fig.4.8 Fracture toughness of specimens sintered at 1650°C

4.4) Microstructure

SEM micrographs are presented in Appendix 4. As shown in Fig 4.10(a) and (b), composition with SPZ has smaller grains than that with GTYS-5. Fig 4.11(a) and (b) show that specimen with GTYS-5 sintered at 1650°C has obviously exaggerated grain growth. On the other hand specimens with SPZ sintered at 1650°C didn't show any exaggerated grain growth. The relationships between average grain size and amount of ZrO_2 are shown in Fig 4.9. It is understood that the effective amount of ZrO_2 to disturb grain growth is over 6 wt% (4 vol.%). Lange et.al reported that 1 and 2.5 vol.% ZrO_2 were not enough for hindrance grain growth, whereas grain growth was disturbed by the addition of 5 vol.% ZrO_2 ⁽¹⁹⁾. Our experimental results coincide with the report. As shown in Fig 4.9, the grain sizes of SPZ added compositions (KM03-05) are slightly smaller than those of GTYS-5 added (KM06-08). The average grain size decreases with increasing ZrO_2 content. Most of ZrO_2 grains are concentrated at the grain boundaries, and are smaller than Al_2O_3 grains, as shown in Fig 4.10(a) and (b).

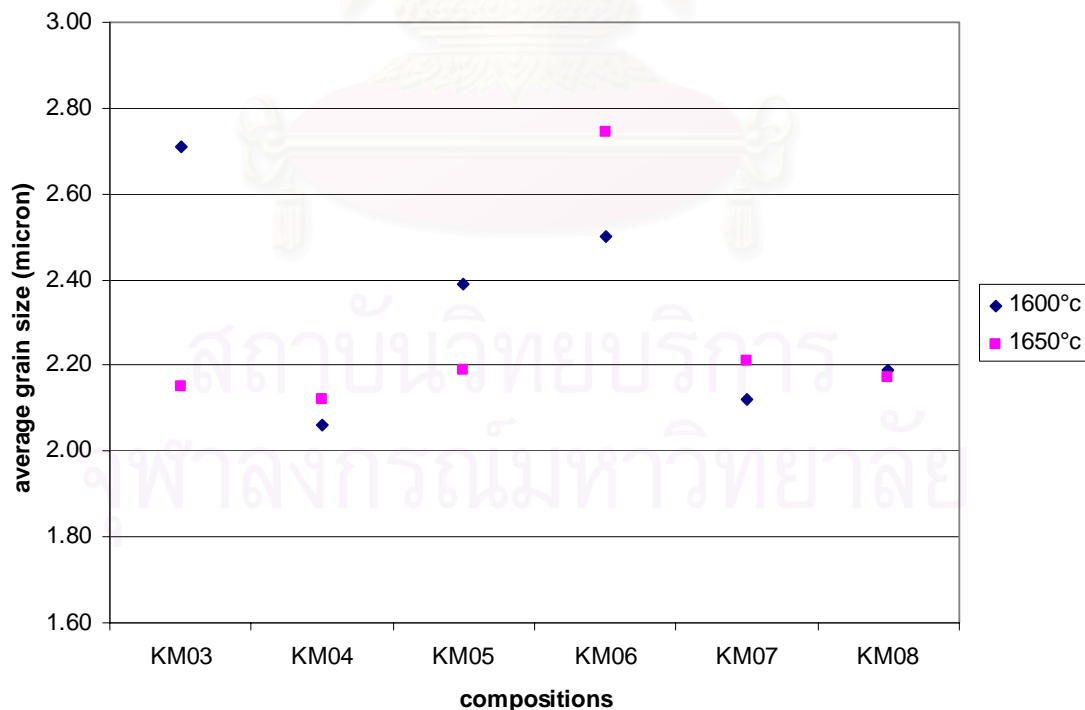


Fig.4.9 Relationship between average grain size and amount of ZrO_2

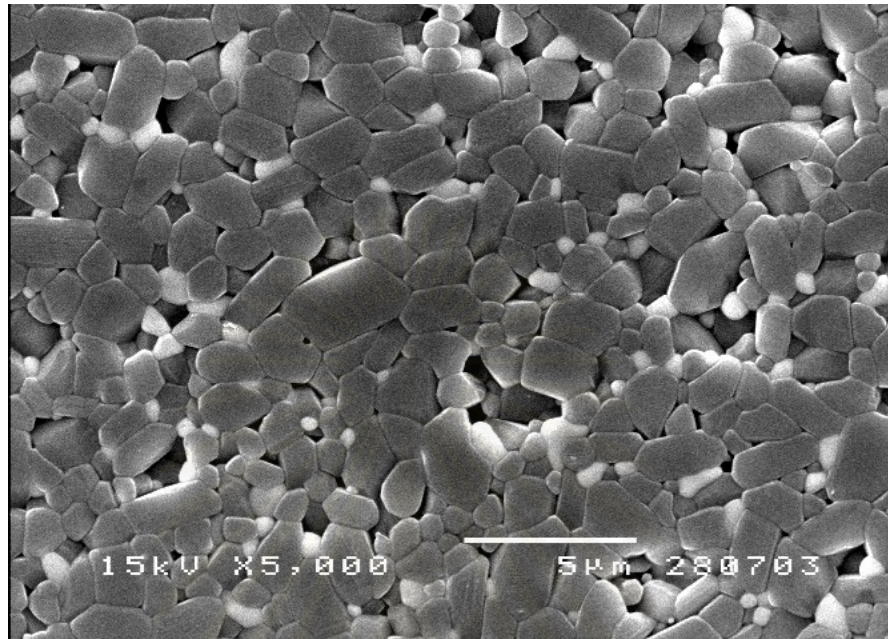


Fig. 4.10(a) SEM micrograph of 6% SPZ added specimen (KM04), sintered at 1600°C

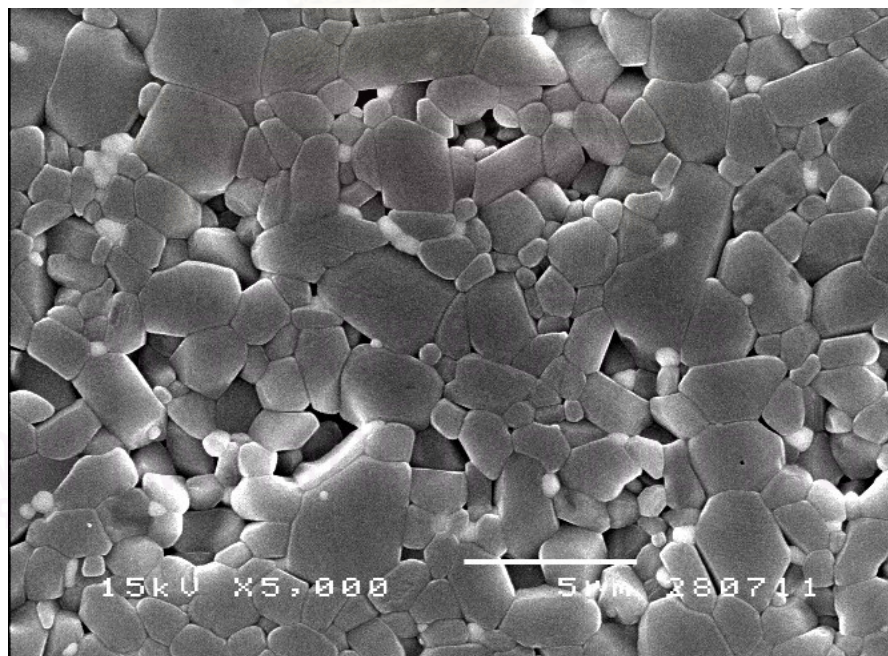


Fig. 4.10(b) SEM micrograph of 6% GTYS-5 added specimen (KM07), sintered at 1600°C



Fig. 4.11(a) SEM micrograph of 6% SPZ added specimen (KM04), sintered at 1650°C

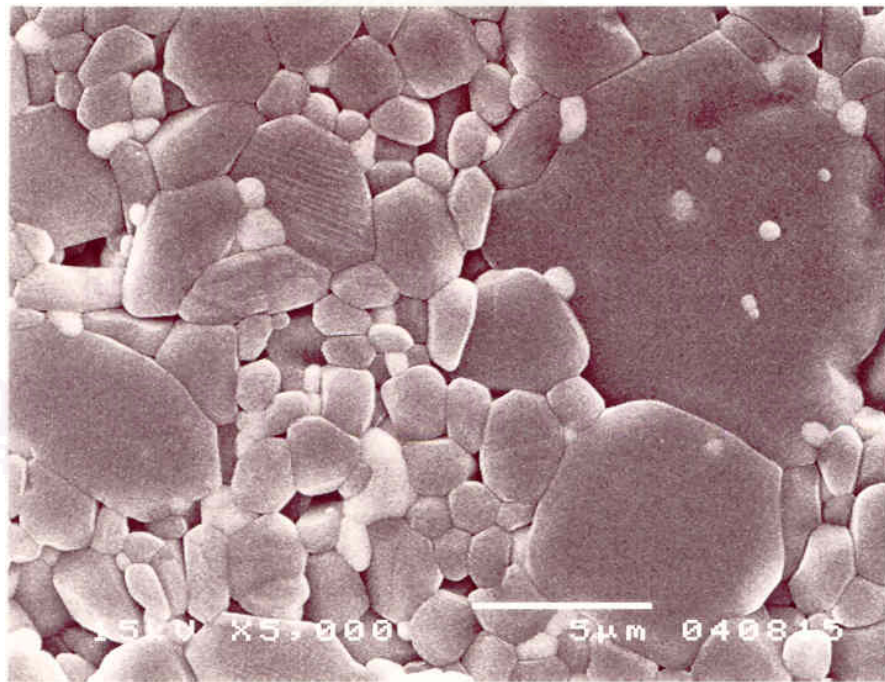


Fig. 4.11(b) SEM micrograph of 6% GTYS-5 added specimen (KM07), sintered at 1650°C

4.5) XRD results of the sintered specimens

XRD patterns of sintered specimens are attached in Appendix 6. The XRD patterns of selected sintered specimens are shown in Fig 4.12. Although either monoclinic and tetragonal ZrO_2 was used as additive, it is found that all the sintered specimens contain $\alpha\text{-Al}_2\text{O}_3$, t-ZrO_2 and small amount of m-ZrO_2 .

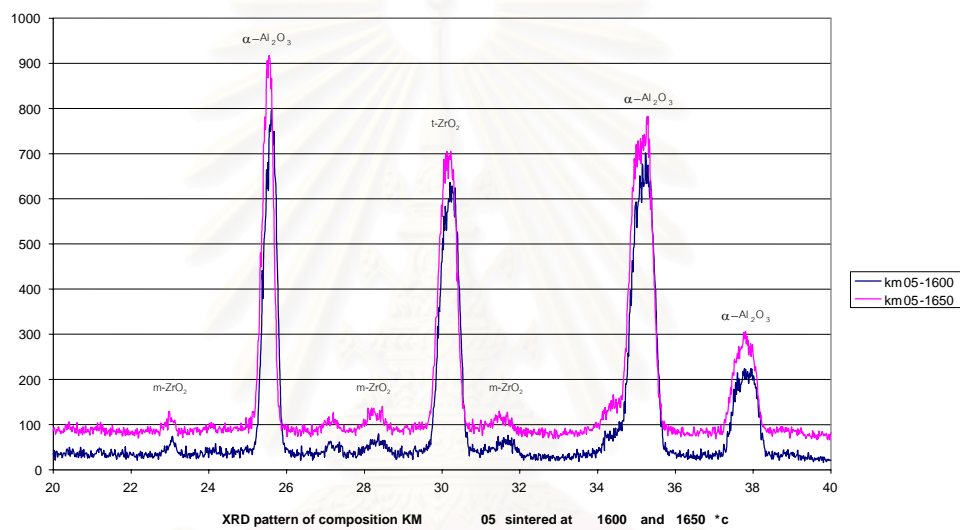


Fig.4.12 XRD patterns of sintered specimens (in pellets) of KM05 at 1600 and 1650°C

SPZ ZrO_2 is monoclinic as shown in Fig 4.3. After sintering, the crystal phase is mainly tetragonal as shown in Fig 4.12. So, it is understood that the $\text{t} \rightarrow \text{m}$ transformation during cooling was hindered by Al_2O_3 matrix. Therefore, the size of SPZ ZrO_2 grains after sintering is thought to be less than the critical size⁽²³⁾.

Chapter 5

Conclusion

The following conclusion can be drawn from the experimental results:

1. Low cost Al_2O_3 , AM-21, can be sintered to almost full density (over 98% of theoretical density) at 1600-1650°C, when it is crushed to less than 1 μm by attrition mill.
2. Acting as effective grain growth inhibitor, the content of ZrO_2 should be over 6 wt% and monoclinic ZrO_2 (SPZ ZrO_2) is more effective than tetragonal one (GTYS-5 ZrO_2). Comparing with MgO, ZrO_2 is more effective.
3. Vickers hardness of Al_2O_3 - ZrO_2 composite is not so sensitive to the increase content of ZrO_2 , hence it does not decrease so much.
4. Fracture toughness of Al_2O_3 - ZrO_2 composite increases a little bit (from 2.76 to 3.5 $\text{MPa}\cdot\text{m}^{1/2}$) with increasing content of ZrO_2 .
5. Although the obtained fracture toughness is less than the target value (5-6 $\text{MPa}\cdot\text{m}^{1/2}$), the Vickers hardness is well above 17 GPa. Hence in summary, Al_2O_3 - ZrO_2 composite with 6-9 wt% ZrO_2 will be suitable as materials for wear resistant media balls due to their fine grain, high hardness (>17 GPa) and appreciable fracture toughness (>3 $\text{MPa}\cdot\text{m}^{1/2}$). Therefore, the best composition for making media ball is the composite with 9 wt% ZrO_2 sintered at 1600°C

สถาบันวิทยบริการ
จุฬาลงกรณ์มหาวิทยาลัย

Chapter 6
Further work

An experiment on testing the real wear resistance of the $\text{Al}_2\text{O}_3\text{-ZrO}_2$ composite with 6-9 wt% ZrO_2 will be performed in the next project.



สถาบันวิทยบริการ
จุฬาลงกรณ์มหาวิทยาลัย

References

1. Wada, S. and Ritter, J., ed. "Effect of hardness and fracture toughness of target materials and impact particles on erosion of ceramic materials," Erosion of Ceramic Materials, Trans Tech Publications, (1992): 51-73.
2. Wada, S. and Watanabe, N. "Solid particle erosion of brittle materials (Part 4): The erosive wear of thirteen kinds of commercial Al_2O_3 ceramics," J. Ceram. Soc. Japan, 95 [9], (1987): 835-40.
3. Wada, S. and Watanabe, N. "Solid particle erosion of brittle materials (Part 6): The erosive wear of Al_2O_3 - ZrO_2 composites," J. Ceram. Soc. Japan, 96 [2], (1988): 111-18.
4. Masaki, H. and Wada, S. "Wear of media balls during the ball milling of Si_3N_4 powder," Ibid, 101 [2], (1993): 221-23.
5. Becher, P.F. and Tennery, V.J. "Fracture toughness of Al_2O_3 - ZrO_2 composites," Fracture Mechanical of Ceramics, Vol. 6, Ed. By R.C. Bract, A.G. Evans, D.P.H. Hasselman and F.F. Lange, Plenum Publishing Corp., New York, (1983): 383-99.
6. Barsoum, M.W. Fundamental of Ceramics. McGraw-Hill, (1997): 430-32.
7. Coble, R.L. and Burke, J.E. "Sintering in Ceramics", In J.E. Burke (Ed), Progress in Ceramic Science. Oxford. Pergamon Press, [2], (1963): 197-251.
8. Kingery, W.D. and Berg, M. "Study of Initial Stage of Sintering Solids by Viscous Flow, Evaporation-Condensation and Self-Diffusion," J. Appl. Phys., 26, (1955): 1205-12.
9. Ashby, M.F. "A First Report on Sintering Diagrams," Acta. Met., 22, (1974): 275-89.
10. Coble, R.L. "Initial Sintering of Alumina and Hematite," J. Am. Ceram. Soc., 41, (1958): 55-62.
11. Coble, R.L. "Sintering Crystalline Solids. I Intermediate and Final Stage Diffusion Models," J. Appl. Phys., 32, (1961): 787-92.
12. Cahoon, H.P. and Christensen, C.J. "Sintering and grain growth of alpha-alumina," J. Am. Ceram. Soc., 39, (1956): 337-44.

13. Coble, R.L. "Sintering crystalline solids. II Experimental test of diffusion models in powder compacts," J. Appl. Phys., 32, (1961): 793-99.
14. Peelen, J.G.J. "Influence of MgO on the evolution of the microstructure of alumina", In Kuczynski, G.C. (Ed). Sintering and catalysis. New York and London. Plenum press, (1975): 443-53.
15. Roy, S.K. and Coble, R.L. "Solubilities of magnesia, titania and magnesium titanate in alumina oxide," J. Am. Ceram. Soc., (1968): 51, 1-6.
16. Heuer, A.H. "The role of MgO in the sintering of alumina," J. Am. Ceram. Soc., 62, (1979): 317-18.
17. Harmer, M.P. and Brook, R.J. "The effect of MgO additions on the kinetics of hot pressing in Al_2O_3 ," J. Mat. Sci., 15, (1980): 3017-24.
18. Claussen, N. "Fracture toughness of Al_2O_3 with an unstabilized ZrO_2 composites," J. Am. Ceram. Soc., 59[1-2], (Jan-Feb 1976): 49-51.
19. Lange, F.F. and Hirlinger, M.M. "Hindranced of Grain Growth in Al_2O_3 by ZrO_2 Inclusions," J. Am. Ceram. Soc., 67 [3], (1984): 164-68.
20. Bocanegra, M.H. and Diaz de la Torre, S. "Phase transitions in zirconium dioxide and related materials for high performance engineering ceramics," J. Mat. Sci., 37, (2002): 4947-71.
21. Stevens, R. Zirconia and zirconia ceramics. for Magnusium Elektron Ltd., Magnusium Elektron Ltd., 17-20.
22. Barsoum, M.W. Fundamental of Ceramics. McGraw-Hill, (1997): 420-24.
23. Claussen, N. "Fracture Toughness of Al_2O_3 with an Unstabilized ZrO_2 Dispersed Phase," J. Am. Ceram. Soc., 59 [2], (1976): 49-51.

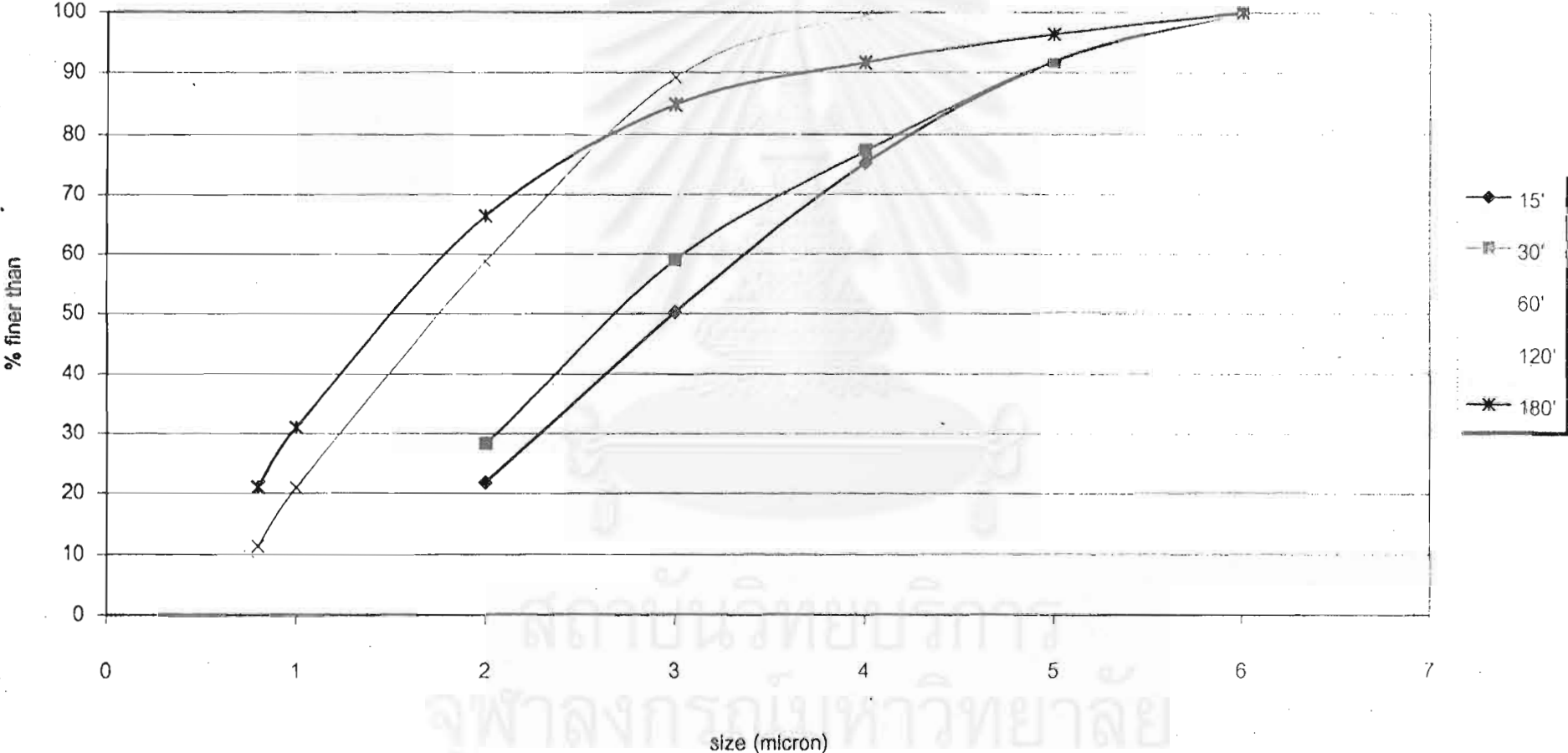


Appendices

สถาบันวิทยบริการ
จุฬาลงกรณ์มหาวิทยาลัย

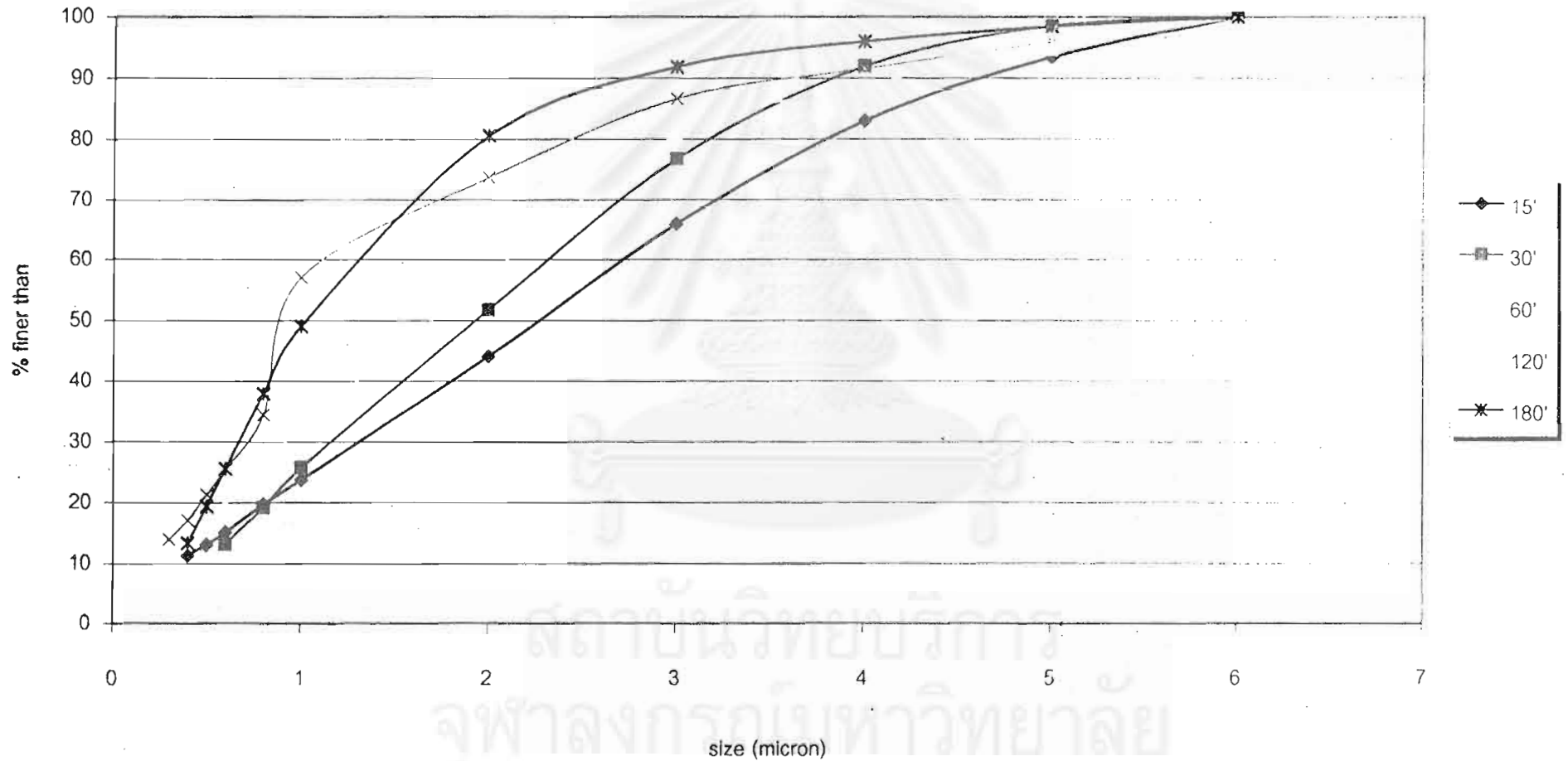
Appendix 1-1

Particle size analysis, AM-21, large-size media balls, 550 rpm



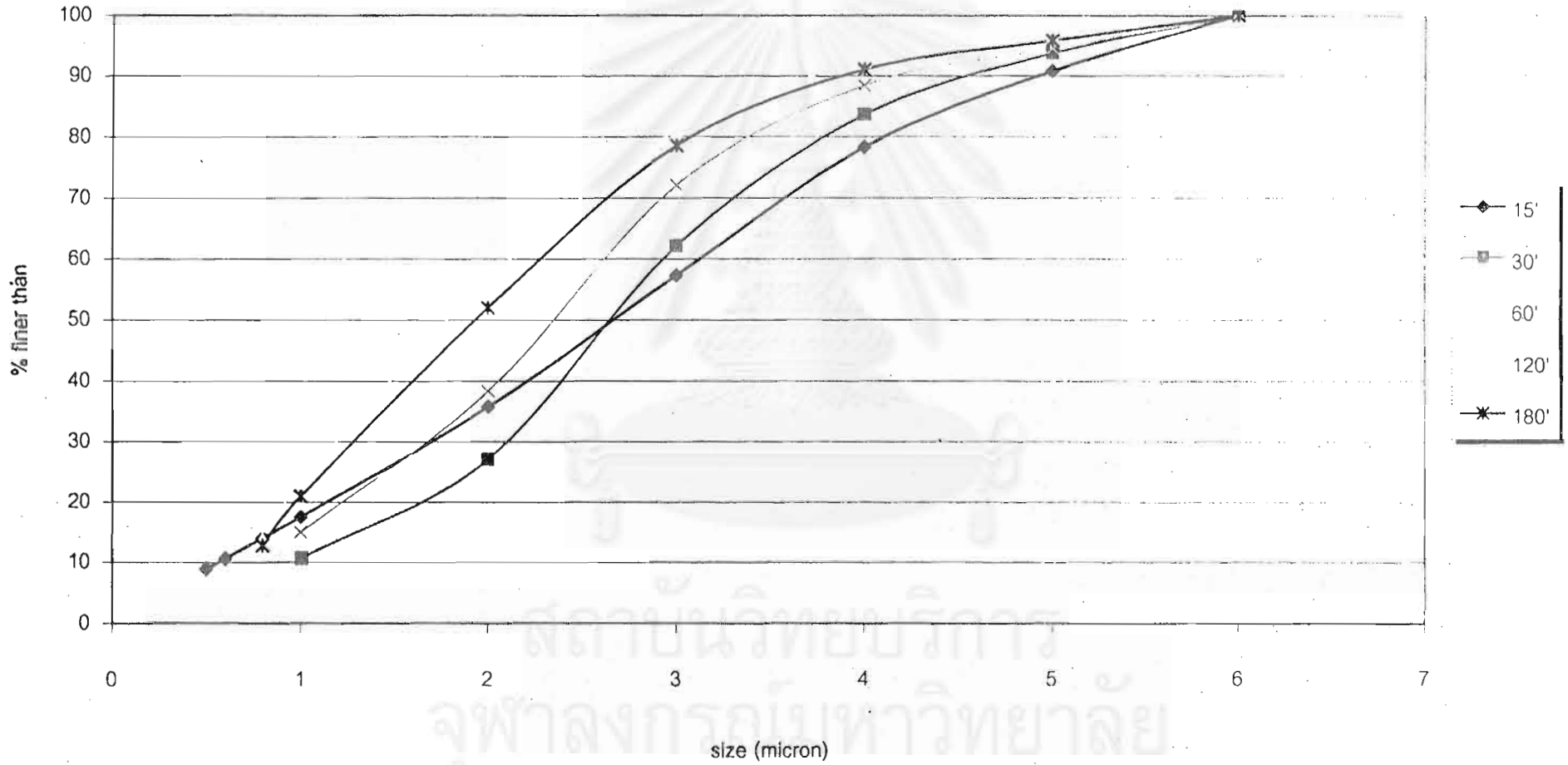
Appendix 1-2

Particle size analysis, AM-21, medium-size media balls, 550 rpm



Appendix 1-3

Particle size analysis, AM-21, small-size media balls, 550 rpm



Appendix 1-4 : AM-21 alumina powder 10hr, medium-size ball, 550rpm

Table 1(a) Particle size distribution data for AM-21 alumina powder ground for 10 hours

	15'	30'	60'	120'	180'	240'	300'	420'	600'
6	100	100	100	100	100	100	100	100	100
5	90.3	94.6	97.5	98.3	98.9	98.8	99.8	99.8	99.4
4	77.8	87.8	93.6	94.9	97.4	97.1	97.6	99.5	98.7
3	57.7	71.3	83.1	89.8	94.6	93.1	94.8	97.1	97.5
2	33.5	42.4	54.2	74.2	85.8	85.4	87.3	91.4	94.7
1	13.4	18.5	24.4	41.5	54.3	56.4	59.4	68.6	80.2
0.8	10.2	13.6	17.4	31.7	42.6	43.9	47.2	56.5	69.4
0.6				21.5	29.1	29.6	30.7	38.2	51.1
0.5				16.9	22.4	22.2	22	25.3	37.6
0.4				12.6	16.1	15.1	12.9		21
0.3					10.2				

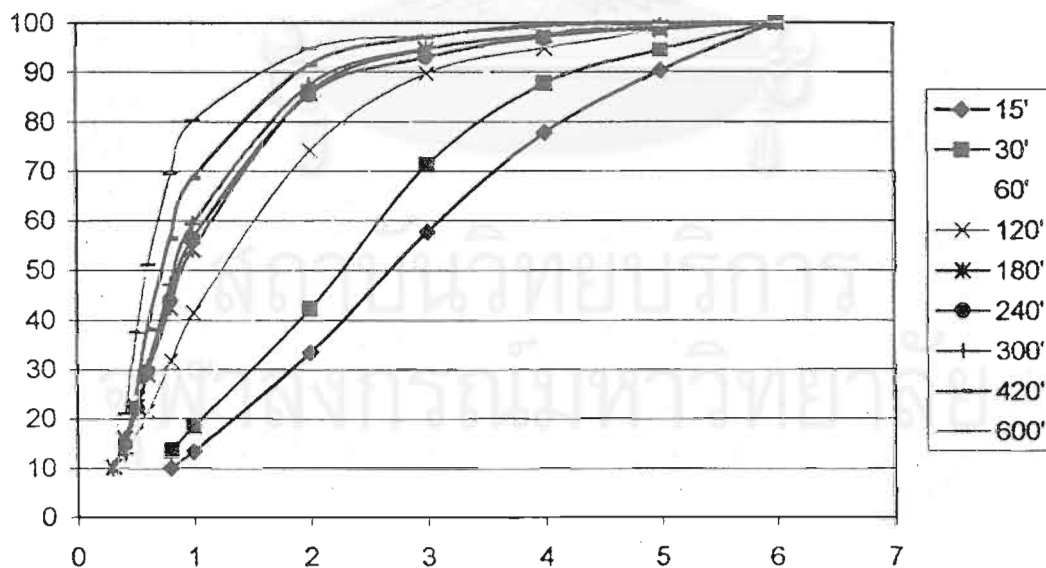


Fig 1(a) Particle size distribution curves for AM-21 alumina powder ground for 10 hours

Appendix 1-5 : SPZ zirconia powder 10hr, medium-size ball, 550rpm

Table 1(b) Particle size distribution data for SPZ zirconia powder ground for 10 hours

	15'	30'	60'	120'	180'	240'	300'	420'	600'
6	100	100	100	100	100	100	100	100	100
5	98.5	98.6	97.8	99.8	100	99.2	99.6	99.1	98.9
4	95.2	96.4	95.5	98.3	97.1	98	99.6	98	98.9
3	90.4	92.8	91.5	95.6	93.4	95.3	98.2	96.2	97.3
2	76	81.1	80.8	88.6	87.6	90.7	95.4	92.2	94.6
1	40	53.6	51.4	63.1	64.3	68.8	78.8	75.7	79.2
0.8	27.2	42.9	41.6	50.2	52	57.2	69.4	65.9	69
0.6	12.9	27.4	28.7	32.5	34.3	40	54.1	52.1	54.9
0.5		17.1	20.3	21.5	22.7	27.9	43.6	42.7	45.6
0.4						13.9	30.4	31	34.2
0.3							16.4	18.6	22
0.2								11.9	11

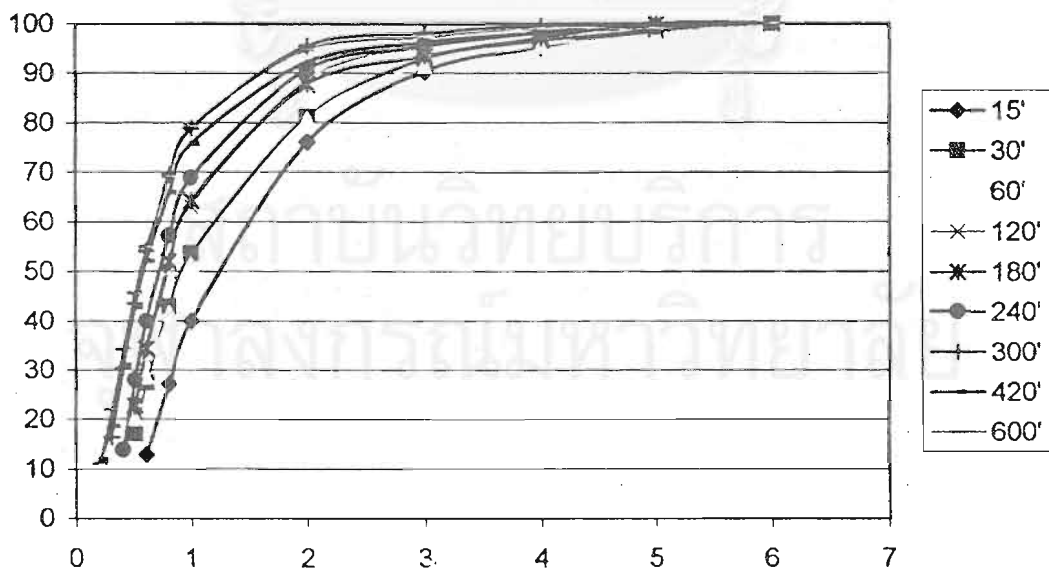


Fig 1(b) Particle size distribution curves for SPZ zirconia powder ground for 10 hours

Appendix 2 : Bulk density, water absorption and % of theoretical density of specimens sintered at 1500, 1550, 1600 and 1650°C.

1500°C

		suspended (g)	saturated (g)	dry (g)	% water absorption	bulk density (g/cm ³)	% of theoretical density	average density
KM01	no.1	1.09	1.52	1.47	5.110	3.42	86.1	85.8
	no.2	1.09	1.51	1.45	5.391	3.40	85.5	
KM02	no.1	1.10	1.51	1.49	2.469	3.60	90.6	90.7
	no.2	1.07	1.47	1.44	2.573	3.60	90.8	
KM03	no.1	1.03	1.43	1.37	5.615	3.41	84.9	85.1
	no.2	1.12	1.56	1.50	5.437	3.42	85.3	
KM04	no.1	1.15	1.56	1.52	3.762	3.62	89.4	89.4
	no.2	1.03	1.41	1.37	3.808	3.62	89.4	
KM05	no.1	1.07	1.46	1.42	3.443	3.64	89.1	89.0
	no.2	1.09	1.49	1.45	3.503	3.64	88.9	
KM06	no.1	1.15	1.58	1.53	4.462	3.50	87.3	87.4
	no.2	1.10	1.51	1.47	4.411	3.51	87.5	
KM07	no.1	1.09	1.49	1.45	3.820	3.57	88.3	88.3
	no.2	1.10	1.51	1.47	3.712	3.58	88.4	
KM08	no.1	1.11	1.53	1.48	4.479	3.56	86.9	86.9
	no.2	1.14	1.57	1.51	4.488	3.55	86.9	

1550°C

		suspended (g)	saturated (g)	dry (g)	% water absorption	bulk density (g/cm ³)	% of theoretical density	average density
KM01	no.1	1.08	1.48	1.46	2.068	3.63	91.3	91.3
	no.2	1.08	1.48	1.46	1.962	3.63	91.3	
KM02	no.1	1.08	1.46	1.46	0.074	3.79	95.6	95.4
	no.2	1.07	1.46	1.46	0.084	3.78	95.2	
KM03	no.1	1.11	1.52	1.48	3.592	3.58	89.4	89.5
	no.2	1.07	1.48	1.44	3.396	3.59	89.6	
KM04	no.1	1.07	1.45	1.45	0.159	3.79	93.7	93.1
	no.2	1.07	1.45	1.44	1.227	3.74	92.5	
KM05	no.1	1.09	1.48	1.47	0.869	3.78	92.4	92.2
	no.2	1.07	1.46	1.45	0.923	3.76	92.0	
KM06	no.1	1.05	1.43	1.43	0.048	3.74	93.3	93.3
	no.2	1.07	1.46	1.46	0.131	3.74	93.2	
KM07	no.1	1.08	1.46	1.46	0.028	3.82	94.3	94.3
	no.2	1.08	1.46	1.45	0.074	3.82	94.3	
KM08	no.1	1.06	1.44	1.43	0.603	3.78	92.4	92.2
	no.2	1.08	1.46	1.45	0.874	3.76	92.0	

1600°C

		suspended (g)	saturated (g)	dry (g)	% water absorption	bulk density (g/cm ³)	% of theoretical density	average density
KM01	no.1	1.09	1.47	1.47	0.055	3.82	96.3	96.7
	no.2	1.05	1.42	1.42	0.076	3.86	97.2	
KM02	no.1	1.08	1.45	1.45	0.074	3.90	98.1	98.1
	no.2	1.11	1.49	1.49	0.063	3.89	98.0	
KM03	no.1	1.08	1.46	1.46	0.101	3.88	96.7	97.0
	no.2	1.10	1.48	1.48	0.027	3.90	97.3	
KM04	no.1	1.10	1.47	1.46	0.073	3.98	98.3	98.7
	no.2	1.10	1.47	1.47	0.036	4.01	99.0	
KM05	no.1	1.13	1.51	1.51	-0.009	4.01	98.2	98.1
	no.2	1.12	1.49	1.49	0.036	4.01	98.0	
KM06	no.1	1.10	1.47	1.47	0.073	3.92	97.6	97.6
	no.2	1.07	1.44	1.44	0.102	3.91	97.6	
KM07	no.1	1.09	1.46	1.45	0.119	3.94	97.4	97.6
	no.2	1.08	1.44	1.44	0.028	3.96	97.7	
KM08	no.1	1.08	1.45	1.45	0.055	3.97	97.0	96.9
	no.2	1.09	1.46	1.46	0.137	3.96	96.8	

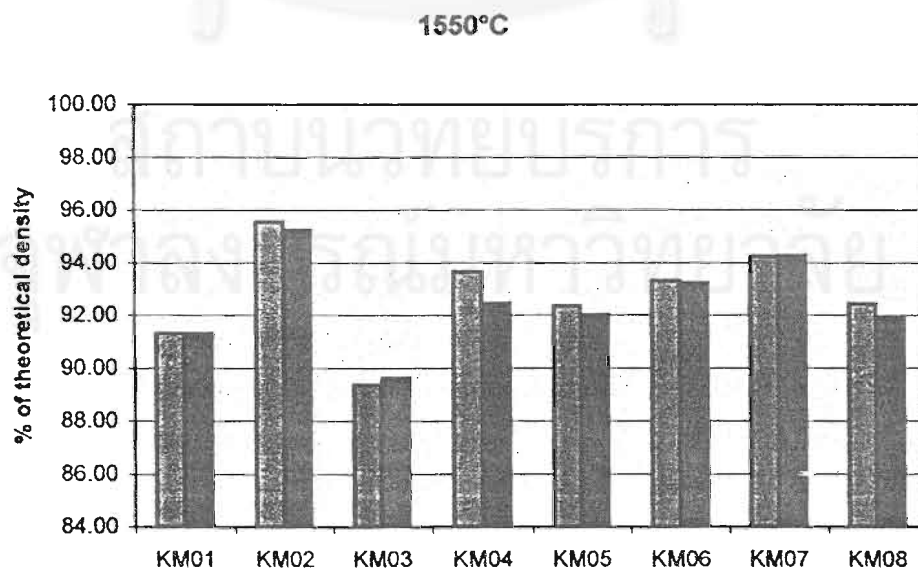
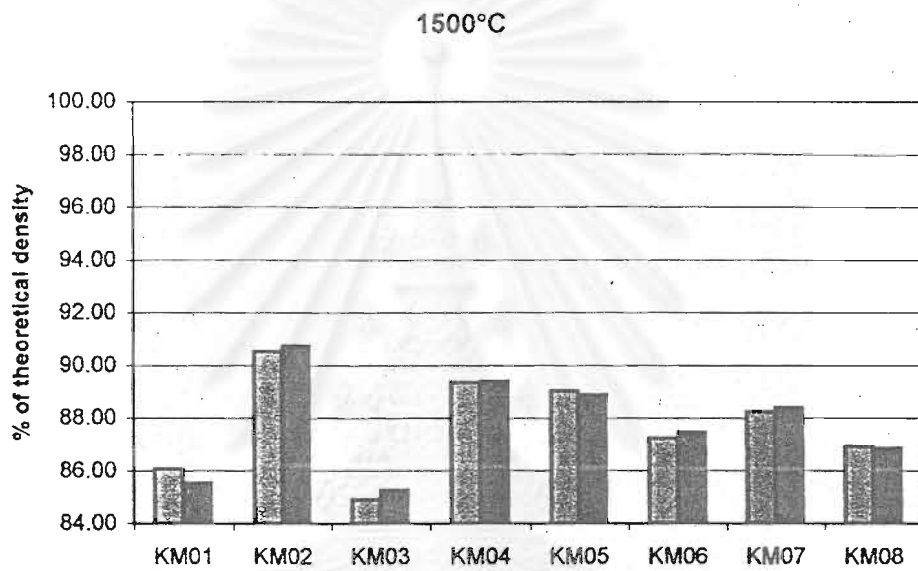
1650°C

		suspended (g)	saturated (g)	dry (g)	% water absorption	bulk density (g/cm ³)	% of theoretical density	average density
KM01	no.1	1.07	1.43	1.43	0.094	3.90	98.1	98.2
	no.2	1.09	1.47	1.47	0.064	3.90	98.3	
KM02	no.1	1.08	1.45	1.45	0.046	3.90	98.2	98.2
	no.2	1.09	1.47	1.47	0.092	3.90	98.2	
KM03	no.1	1.09	1.46	1.46	0.110	3.96	98.8	98.9
	no.2	1.08	1.45	1.45	0.065	3.97	98.9	
KM04	no.1	1.10	1.47	1.46	0.100	4.05	99.9	100.0
	no.2	1.12	1.49	1.49	0.089	4.05	100.0	
KM05	no.1	1.09	1.45	1.45	0.064	4.05	99.0	99.0
	no.2	1.07	1.42	1.42	0.047	4.05	99.0	
KM06	no.1	1.07	1.43	1.43	0.075	3.93	98.1	98.0
	no.2	1.08	1.45	1.45	0.102	3.92	97.9	
KM07	no.1	1.09	1.45	1.45	0.166	3.94	97.4	97.5
	no.2	1.08	1.45	1.45	0.074	3.95	97.6	
KM08	no.1	1.10	1.47	1.47	0.091	3.98	97.3	97.2
	no.2	1.06	1.41	1.41	0.104	3.97	97.1	

Appendix 2-1 : % of theoretical density of specimens sintered at 1500, 1550, 1600 and 1650°C.

1500°C	KM01	86.1	85.5
	KM02	90.6	90.8
	KM03	84.9	85.3
	KM04	89.4	89.4
	KM05	89.1	88.9
	KM06	87.3	87.5
	KM07	88.3	88.4
	KM08	86.9	86.9

1550°C	KM01	91.3	91.3
	KM02	95.6	95.2
	KM03	89.4	89.6
	KM04	93.7	92.5
	KM05	92.4	92.0
	KM06	93.3	93.2
	KM07	94.3	94.3
	KM08	92.4	92.0

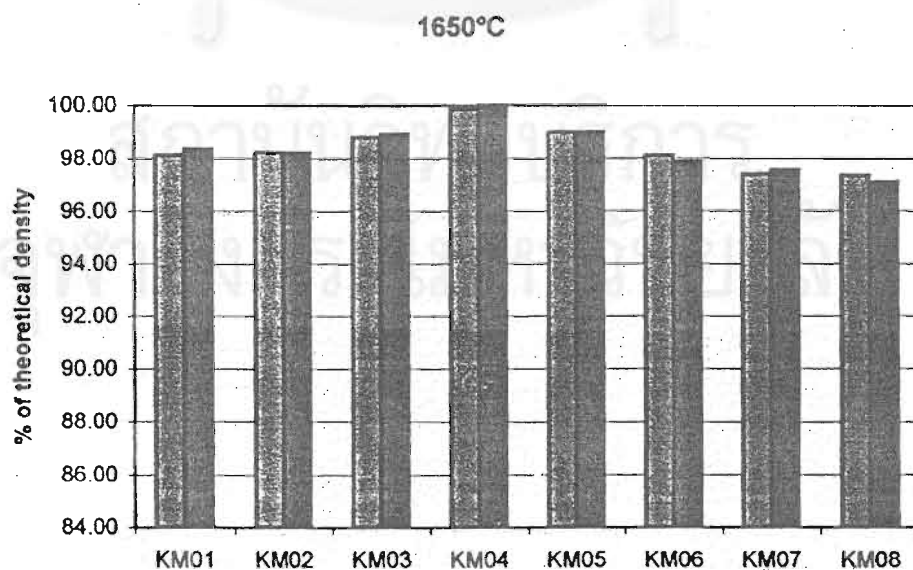
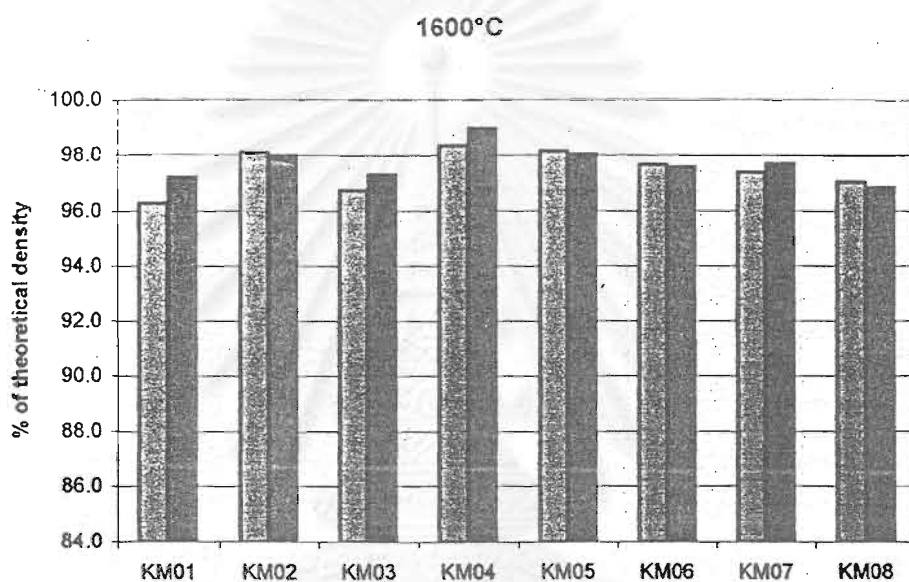


1600°C

KM01	96.3	97.2
KM02	98.1	98.0
KM03	96.7	97.3
KM04	98.3	99.0
KM05	98.2	98.0
KM06	97.6	97.6
KM07	97.4	97.7
KM08	97.0	96.8

1650°C

KM01	98.1	98.3
KM02	98.2	98.2
KM03	98.8	98.9
KM04	99.9	100.0
KM05	99.0	99.0
KM06	98.1	97.9
KM07	97.4	97.6
KM08	97.3	97.1



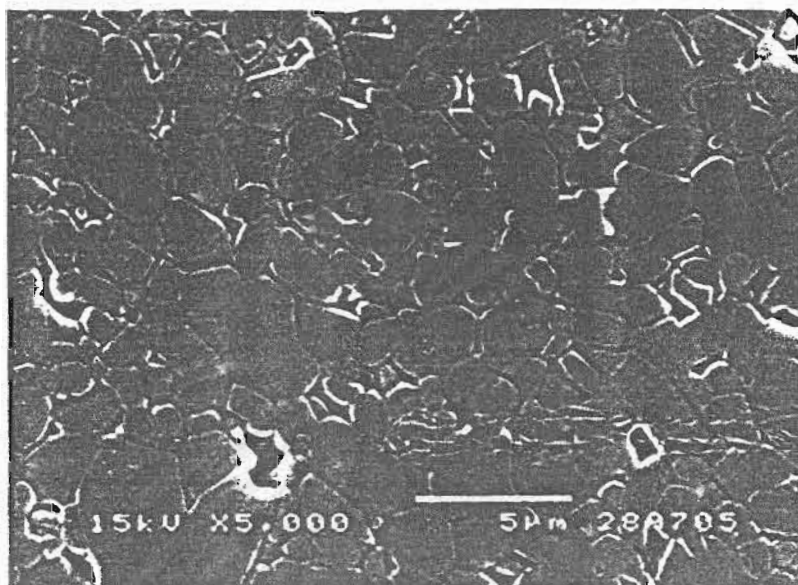
Appendix 3 : Vickers hardness and fracture toughness of specimens sintered at 1600 and 1650°C

1600°C

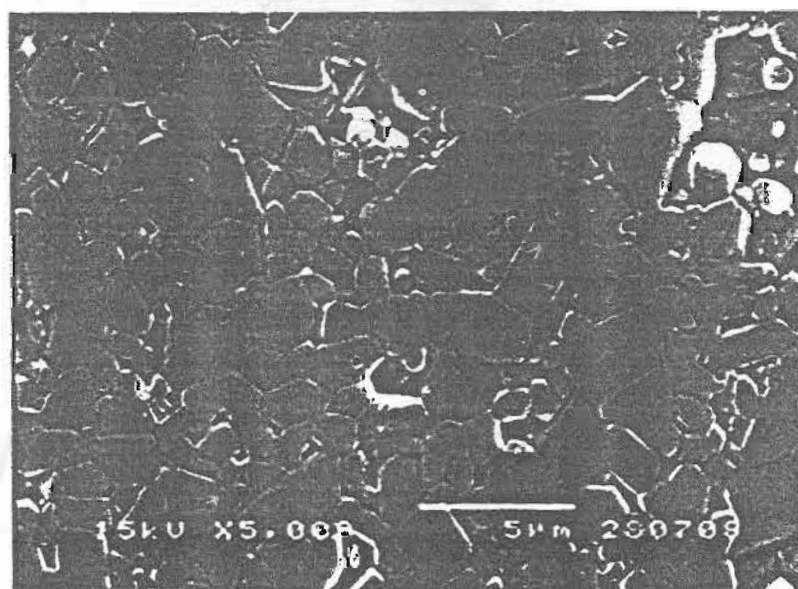
Specimen	Micron				Hv (Gpa)	Kic (MPam ^{1/2})
	Diagonal X	Diagonal Y	Crack X	Crack Y		
km01	103.33	104.24	319.38	319.86	16.88	2.62
	106.38	105.62	288.52	316.33	16.19	2.70
	105.57	105.05	295.81	288.62	16.40	2.87
	103.10	103.71	291.71	0.00	17.01	2.86
	102.67	102.38	298.76	308.19	17.30	2.72
average					16.76	2.76
km02	102.19	102.38	288.00	293.09	17.38	2.81
	103.33	103.81	238.29	251.14	16.95	3.33
	101.19	102.76	295.90	291.67	17.49	2.78
	103.95	104.43	293.86	284.43	16.75	2.91
	101.95	100.67	295.86	308.43	17.72	2.70
average					17.26	2.91
km03	105.05	103.67	306.19	264.81	16.70	2.95
	105.95	105.43	307.48	300.14	16.28	2.81
	104.48	105.00	283.67	280.86	16.58	2.99
	104.57	104.62	281.67	271.43	16.62	3.05
	105.33	104.95	275.43	274.90	16.45	3.08
average					16.53	2.98
km04	102.86	103.33	267.38	284.14	17.11	3.01
	102.48	102.48	277.33	277.19	17.32	2.98
	100.38	101.86	299.43	310.24	17.79	2.72
	100.43	100.67	291.05	280.00	17.99	2.90
	102.05	101.19	265.71	266.76	17.61	3.08
average					17.56	2.94
km05	99.71	100.10	265.43	269.33	18.22	3.01
	103.05	103.33	303.57	270.62	17.08	2.90
	101.48	99.52	287.62	261.57	18.01	3.10
	100.57	99.86	286.81	263.38	18.11	3.07
	101.19	101.86	282.19	277.57	17.64	2.90
average					17.81	3.00
km06	101.48	101.76	264.57	259.19	17.61	3.13
	100.29	104.38	271.86	267.67	17.37	3.06
	98.71	99.29	268.24	261.52	18.56	3.01
	100.19	99.76	267.05	241.81	18.19	3.17
	99.10	99.14	257.38	258.95	18.51	3.11
average					18.05	3.10
km07	103.52	104.38	287.90	287.52	16.83	2.91
	101.71	102.10	293.76	273.81	17.51	2.90
	100.48	102.00	290.57	293.95	17.74	2.79
	103.29	103.29	279.76	293.00	17.05	2.98
	104.14	104.43	295.57	298.52	16.72	2.85
average					17.17	2.88
km08	106.29	103.05	269.90	267.43	16.60	3.14
	106.48	104.14	284.38	264.38	16.40	3.09
	103.48	103.57	267.33	268.71	16.97	3.11
	103.71	103.24	256.48	255.05	16.98	3.26
	103.38	102.90	261.48	262.67	17.09	3.17
average					16.81	3.16

1650°C

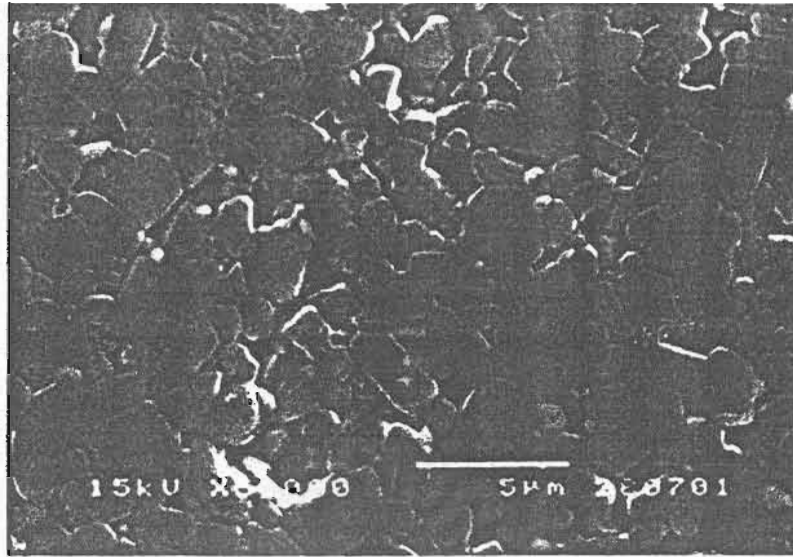
Specimen	Micron				Hv (Gpa)	Kic (MPam ^{1/2})
	Diagonal X	Diagonal Y	Crack X	Crack Y		
km01	105.24	104.96	269.38	269.47	16.49	3.14
	104.53	103.87	268.95	269.16	16.74	3.12
	105.81	104.86	269.45	269.88	16.44	3.14
	105.94	105.26	270.19	272.31	16.29	3.14
	104.67	104.59	271.94	269.41	16.62	3.12
average					16.53	3.13
km02	104.56	103.43	278.42	280.48	16.85	3.00
	102.36	103.75	283.49	281.57	17.06	2.95
	104.97	104.23	282.36	282.97	16.65	2.98
	103.54	103.28	283.49	281.27	16.96	2.96
	103.27	104.24	284.05	282.91	16.90	2.97
average					16.85	2.97
km03	102.67	103.08	270.91	271.95	17.22	3.05
	103.45	102.06	270.94	270.88	17.17	3.06
	102.51	103.49	271.81	270.96	17.13	3.06
	103.94	102.86	272.83	272.94	17.03	3.05
	103.97	101.79	273.86	273.19	17.15	3.04
average					17.13	3.06
km04	103.96	102.45	264.25	266.13	17.07	3.14
	103.40	101.98	254.91	240.38	17.25	3.25
	103.68	102.36	247.93	227.74	17.14	3.35
	102.45	101.13	258.11	233.21	17.55	3.52
	103.59	103.40	259.53	243.30	16.98	3.32
average					17.25	3.31
km05	101.23	101.60	291.23	276.89	17.68	2.88
	102.08	102.17	281.89	293.77	17.44	2.86
	102.36	102.64	273.49	259.25	17.31	3.19
	102.26	102.26	273.49	254.53	17.39	3.24
	103.59	102.92	238.21	250.47	17.06	3.50
average					17.38	3.20
km06	107.74	107.36	295.38	281.60	15.72	3.01
	105.28	106.79	272.55	258.87	16.17	3.22
	104.34	104.06	261.60	252.64	16.75	3.27
	107.92	104.25	274.72	216.70	16.16	3.48
	105.09	106.04	256.04	270.38	16.32	3.32
average					16.23	3.26
km07	104.06	103.96	251.23	260.66	16.81	3.28
	104.53	103.40	233.30	233.11	16.83	3.59
	102.55	101.04	237.93	211.13	17.55	3.66
	105.19	104.53	267.27	241.98	16.54	3.16
	104.91	103.40	219.72	238.68	16.77	3.82
average					16.90	3.50
km08	101.42	102.92	238.02	259.05	17.42	3.46
	103.11	103.68	291.51	228.21	17.01	3.21
	101.79	101.13	226.89	229.15	17.67	3.59
	101.42	103.49	231.42	223.49	17.33	3.70
	103.21	101.60	295.94	248.30	17.34	3.03
average					17.35	3.40



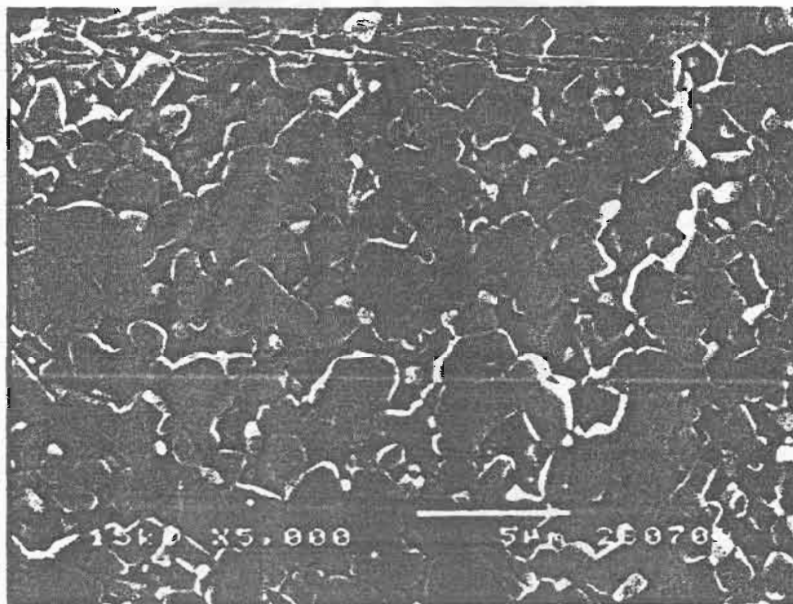
Micrograph of KM01 sintered at 1600°C



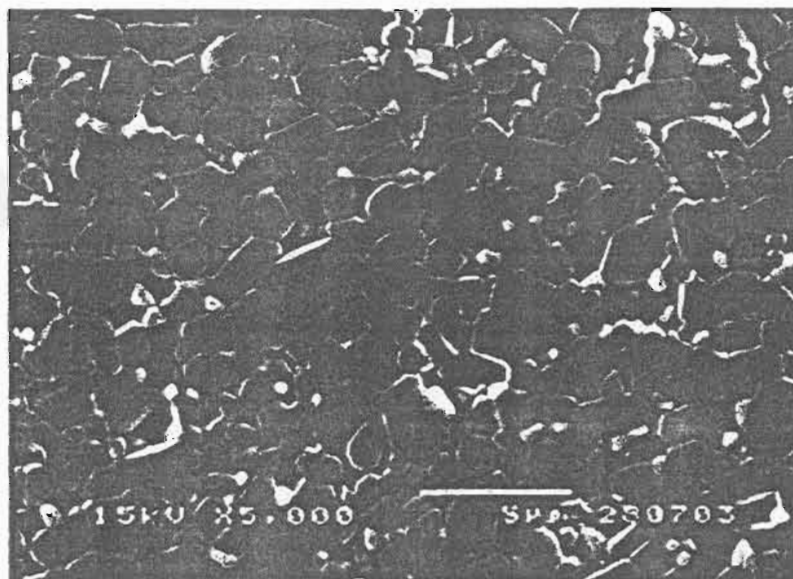
Micrograph of KM02 sintered at 1600°C



KM03

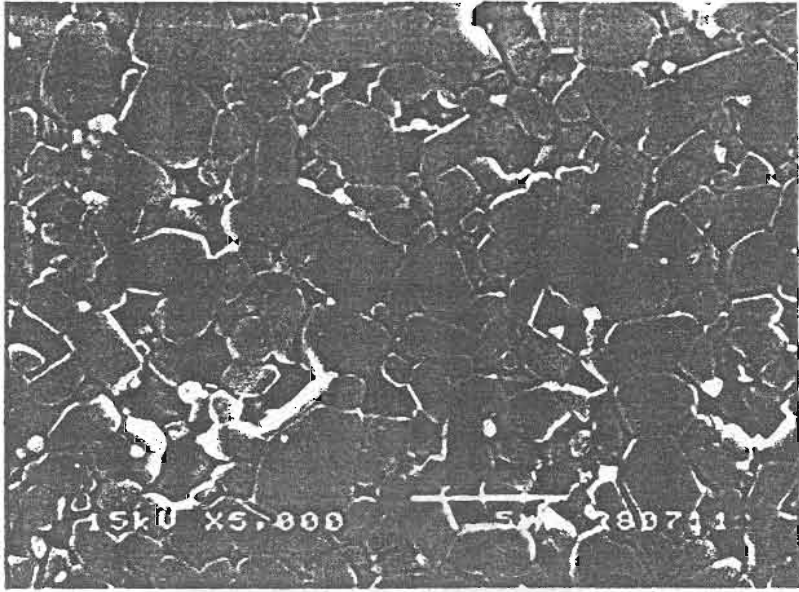


KM04

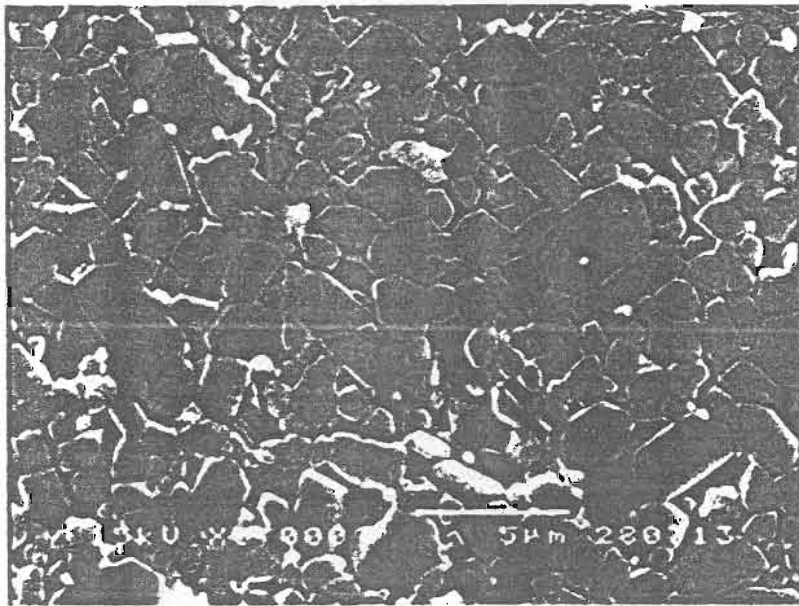


KM05

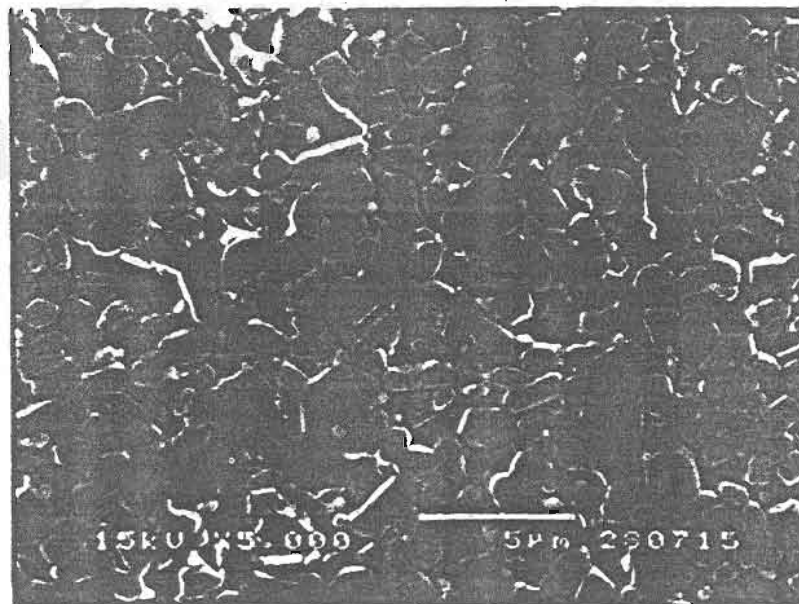
Micrographs of KM03 - 05 sintered at 1600°C (white spots are zirconia)



KM06

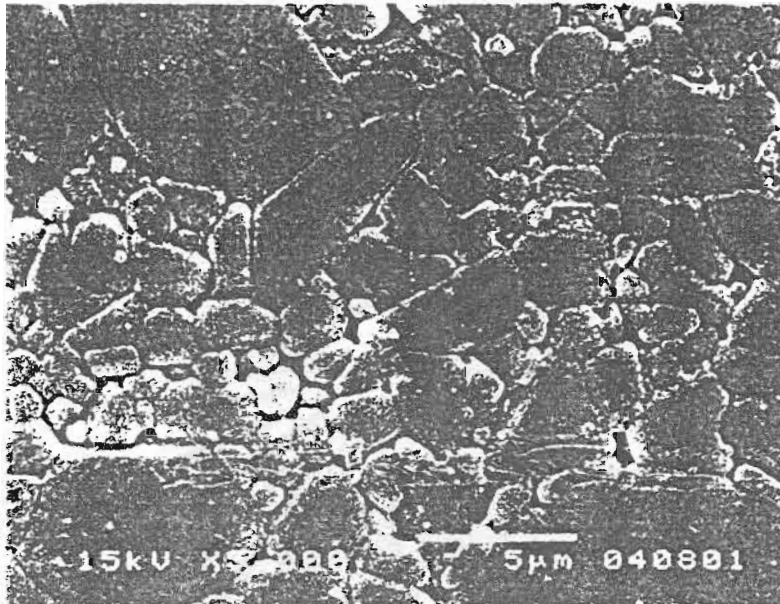


KM07

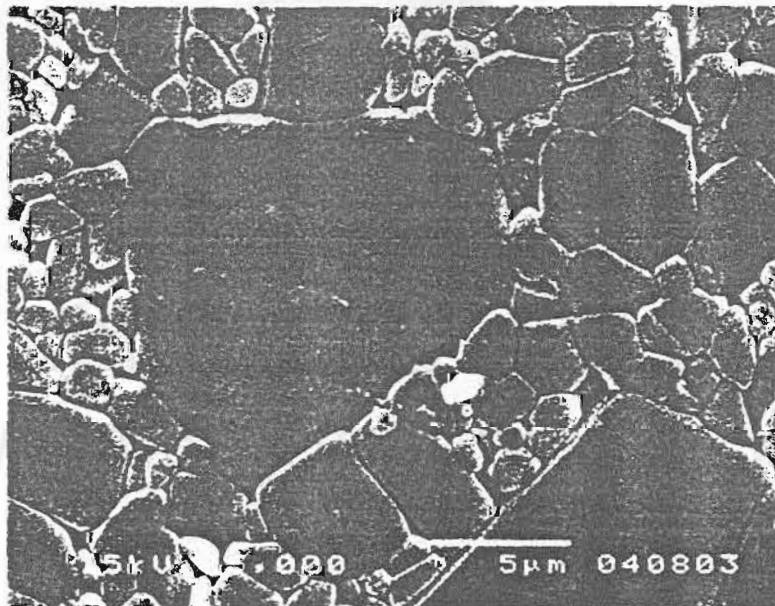


KM08

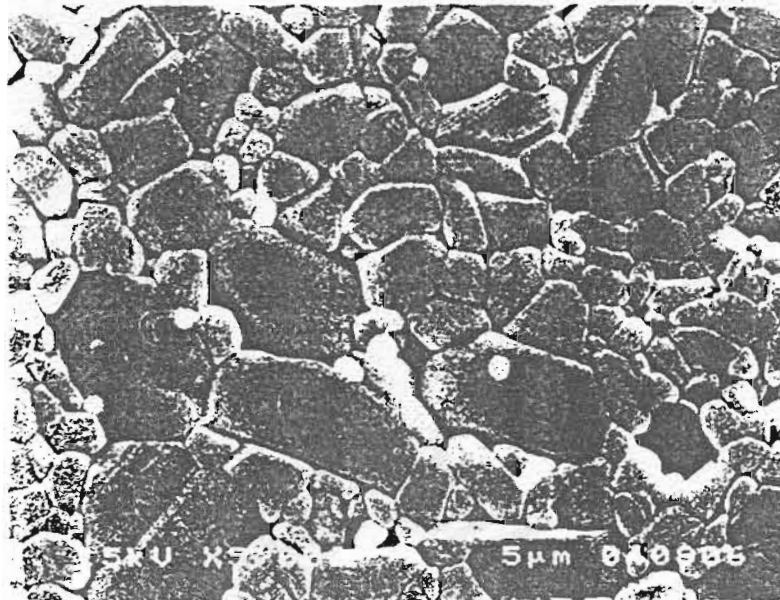
Micrographs of KM06 - 08 sintered at 1600°C (white spots are zirconia)



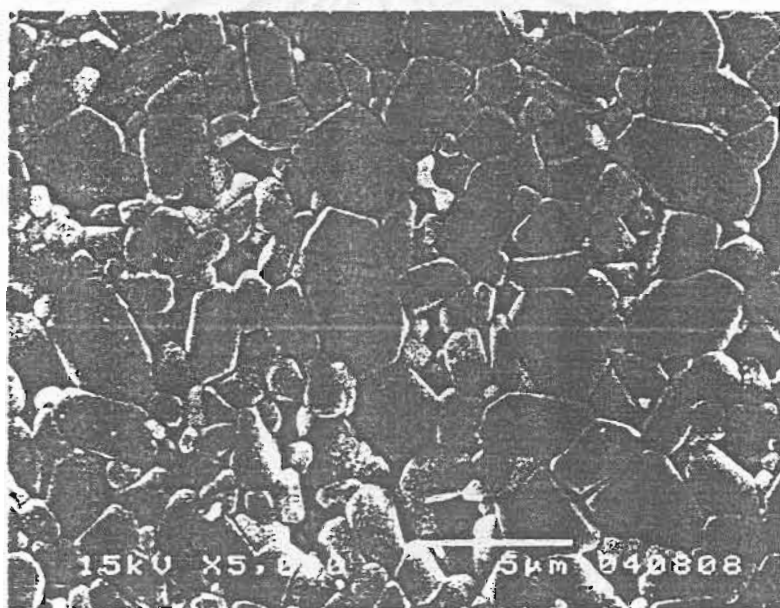
Micrograph of KM01 sintered at 1650°C



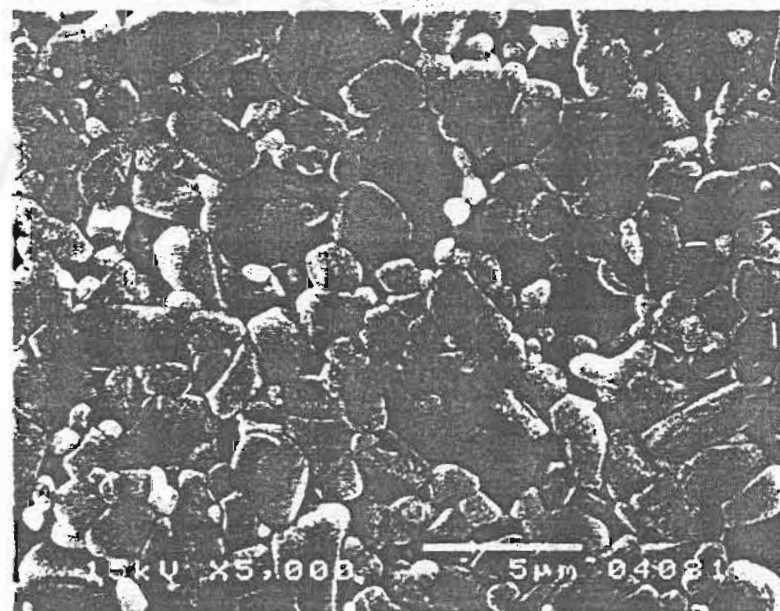
Micrograph of KM02 sintered at 1650°C



KM03

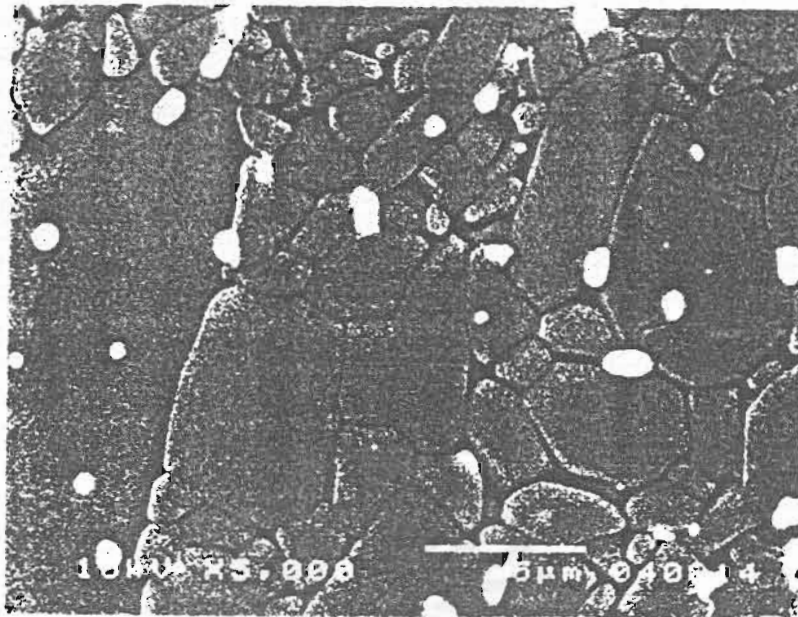


KM04

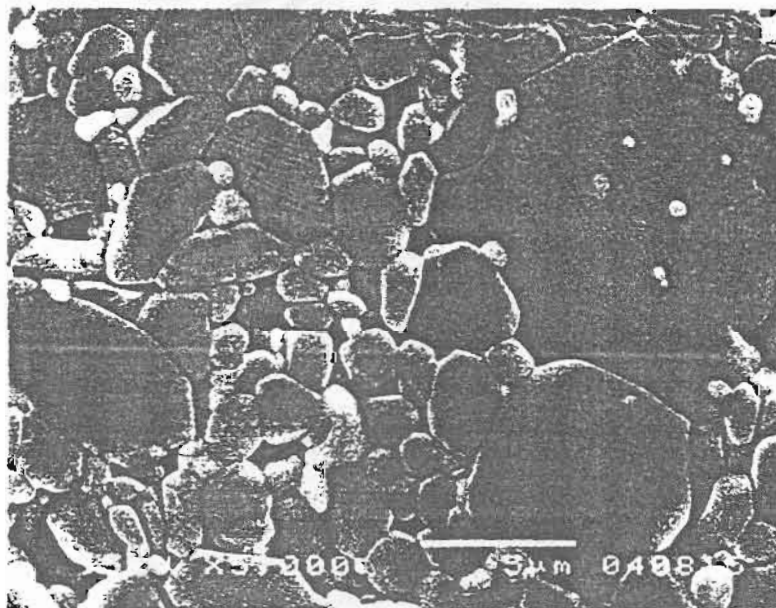


KM05

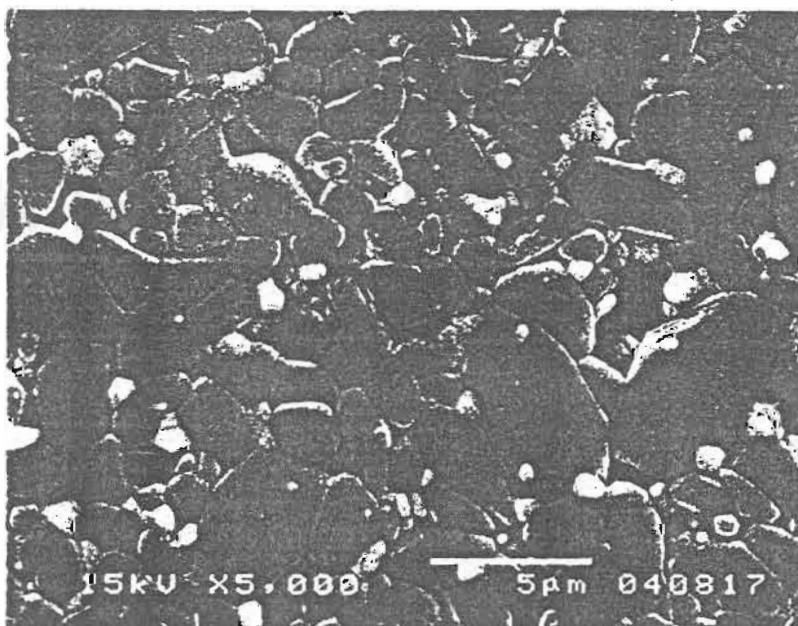
Micrographs of KM03 - 05 sintered at 1650°C (white spots are zirconia)



KIM06



KIM07



KIM08

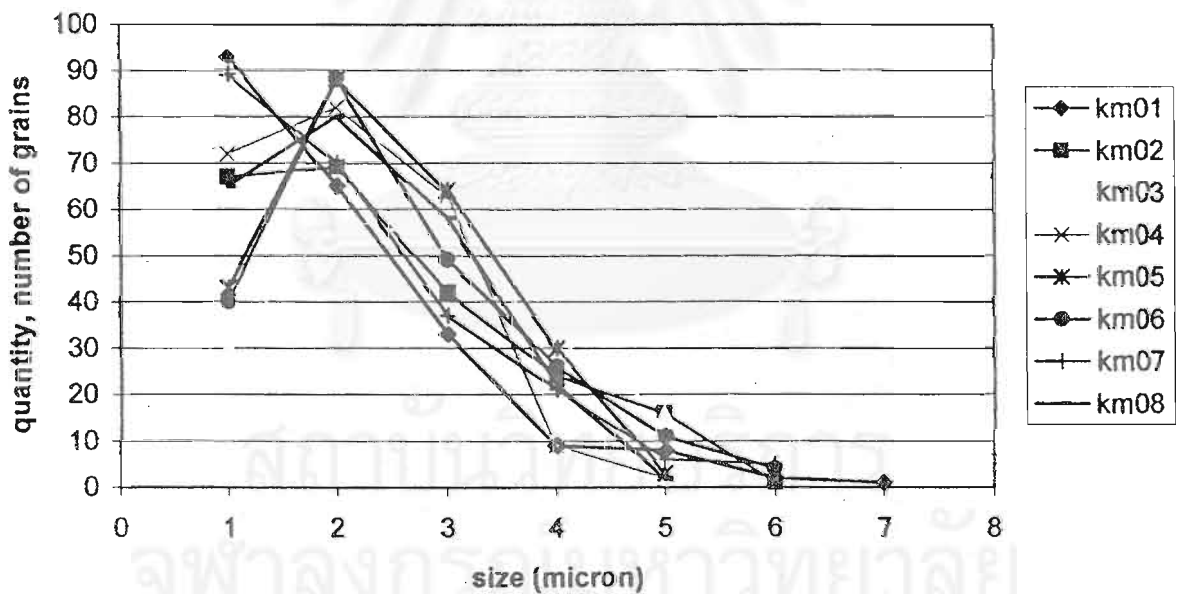
Micrographs of KIM06 - 08 sintered at 1650°C (white spots are zirconia)

Appendix 5-1 : Grain size measurement

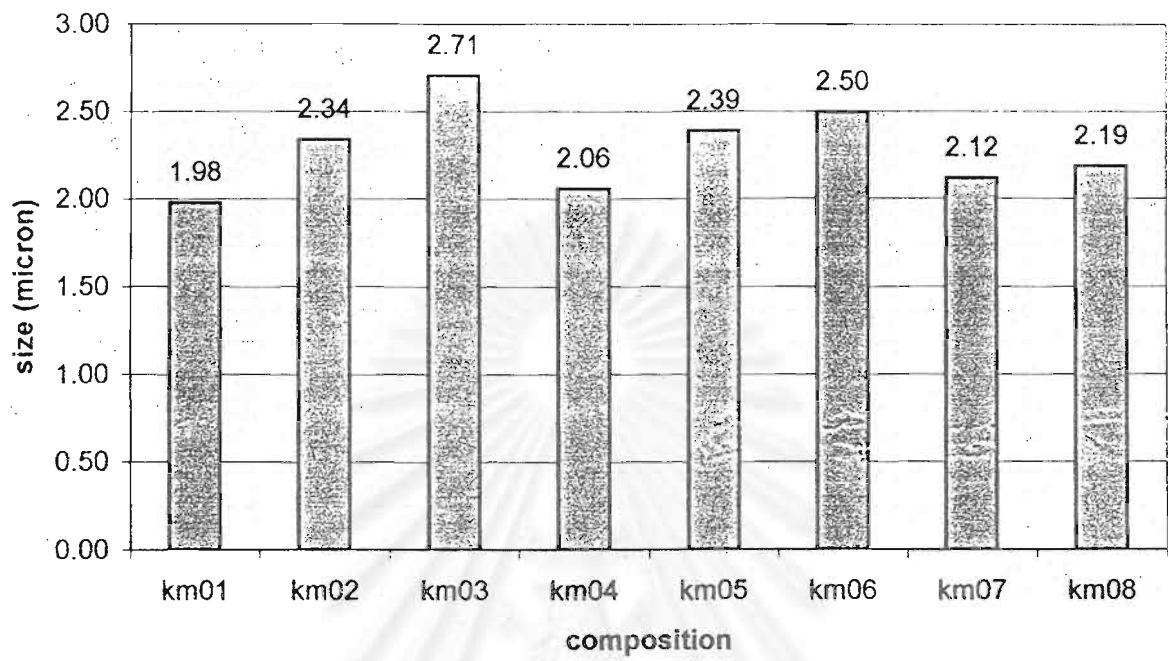
Table 1(a) Average grain size of specimens sintered at 1600°C.

size (μm)	km01	km02	km03	km04	km05	km06	km07	km08
1	93	67	30	72	43	40	89	65
2	65	69	58	82	88	88	70	80
3	33	42	53	63	64	49	37	58
4	9	24	32	9	30	26	21	22
5	8	16	16	2	3	11	6	2
6	2	1				4	5	
7	1							
total	211	219	189	228	228	218	228	227
Average grain size(μm)	1.98	2.34	2.71	2.06	2.39	2.50	2.12	2.19

grain size distribution curves



average grain size

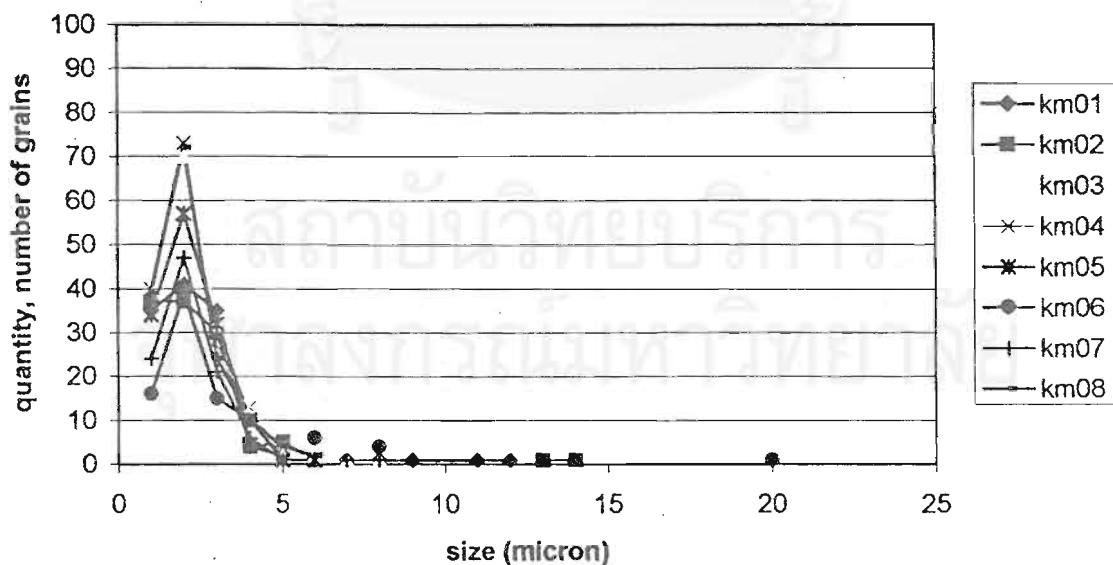


Appendix 5-2 : Grain size measurement

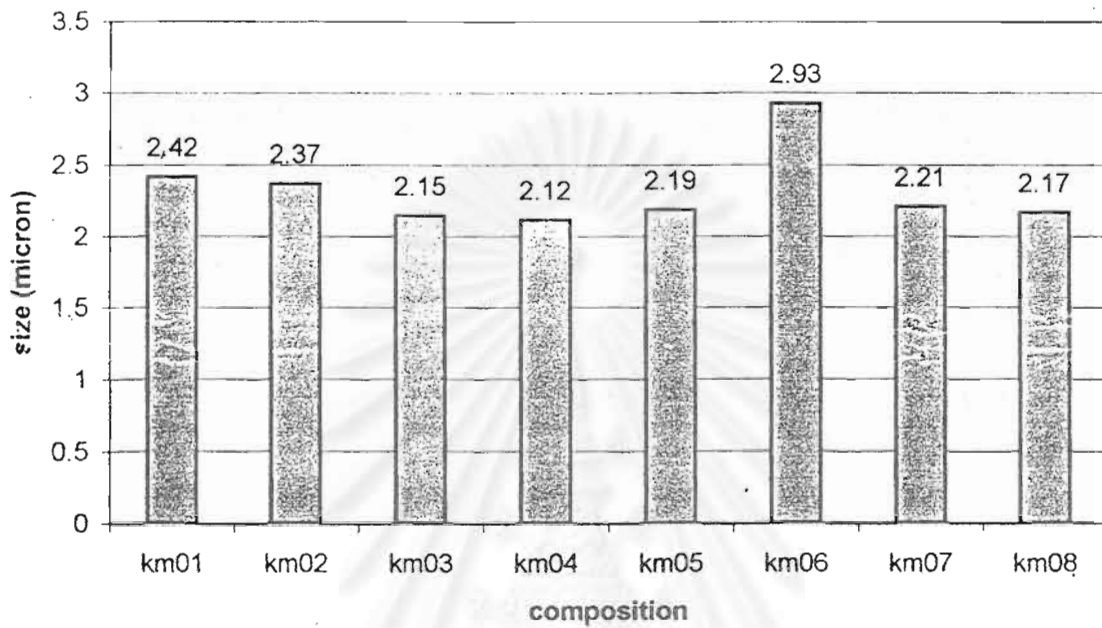
Table 1(b) Average grain size of specimens sintered at 1650°C.

size (μm)	km01	km02	km03	km04	km05	km06	km07	km08
1	35	37	63	40	34	16	24	39
2	41	37	70	73	57	39	47	72
3	35	30	32	26	32	15	21	24
4	4	4	11	13	10	10	6	10
5	2	5	2	1	1		1	4
6		1	2	1	1	6		2
7	1		1				1	
8	1		1			4	1	
9	1							
11	1							
12	1						1	
13		1						
14		1						
20						1		
total	122	116	177	154	135	91	102	151
Average grain size(μm)	2.42	2.37	2.15	2.12	2.19	2.93	2.21	2.17

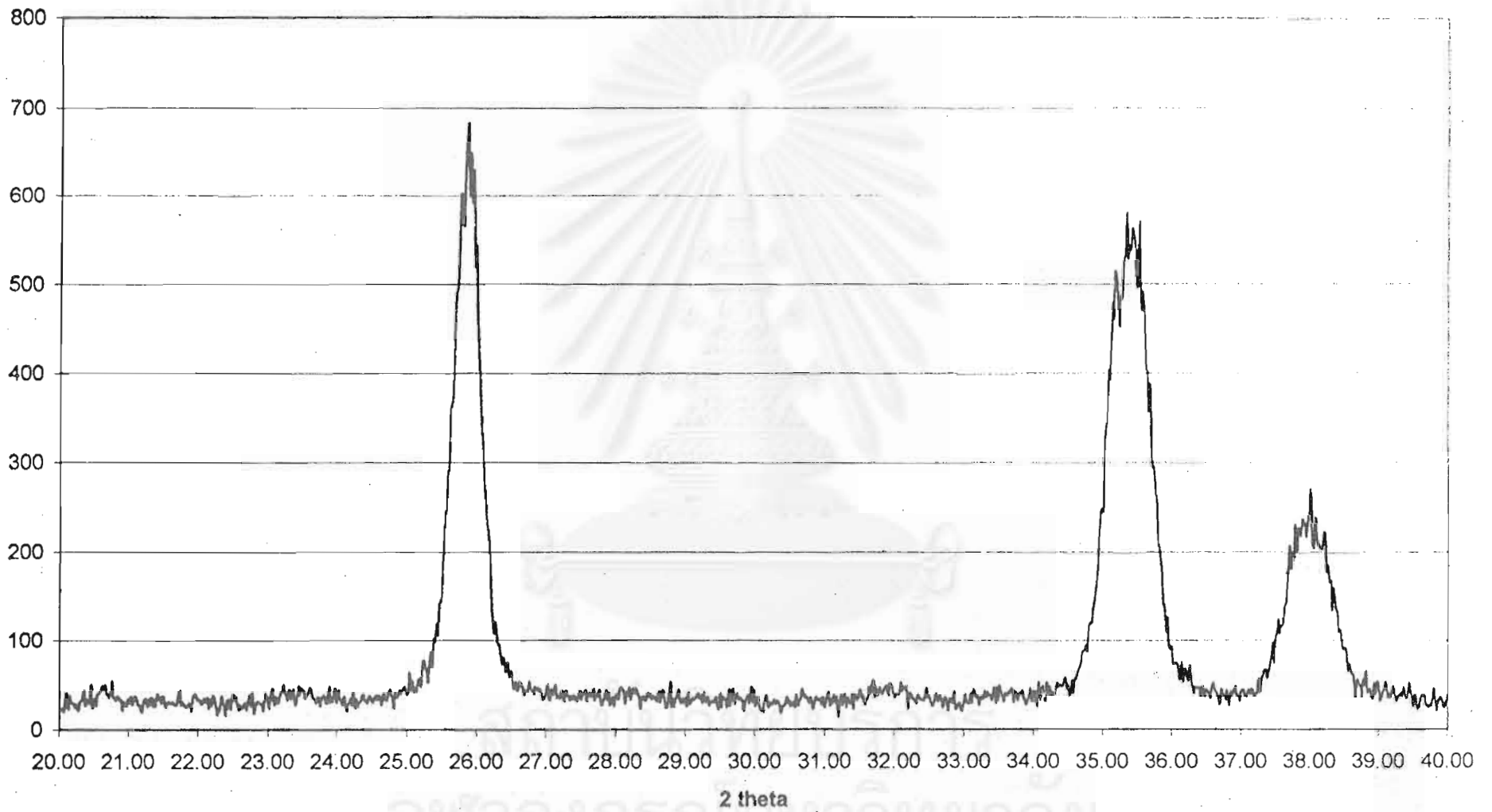
grain size distribution curves



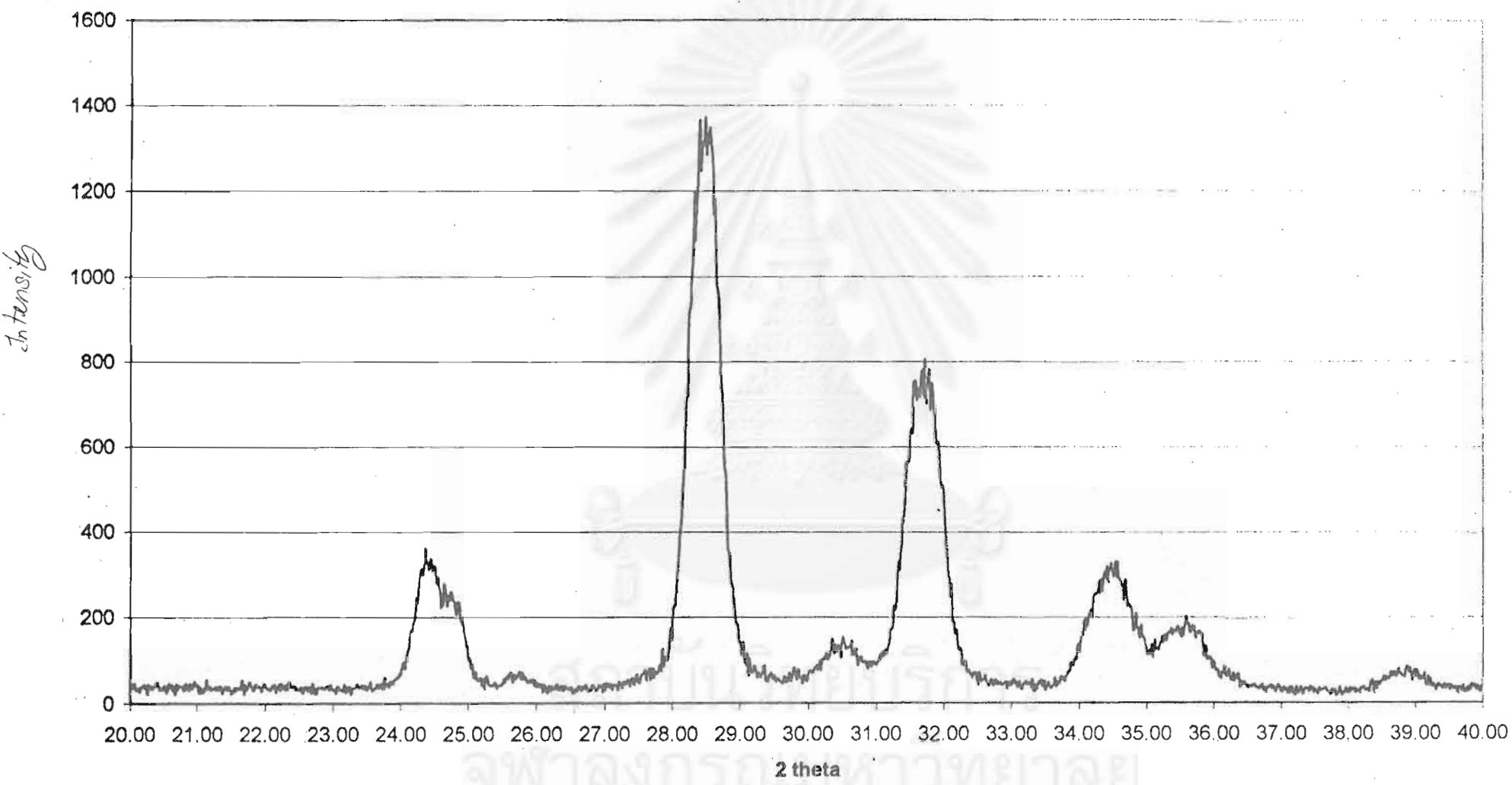
average grain size



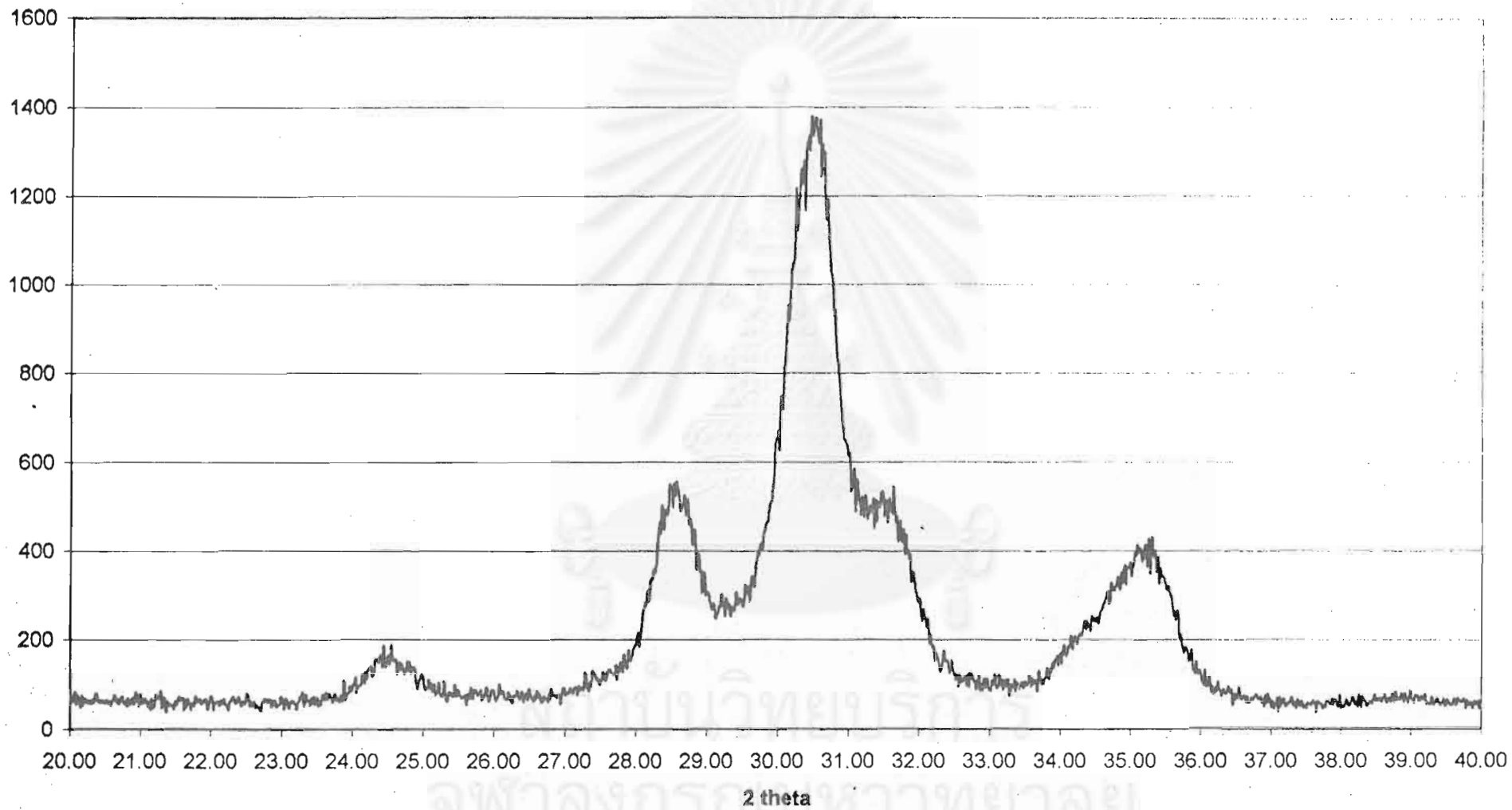
สถาบันวิทยบริการ
จุฬาลงกรณ์มหาวิทยาลัย



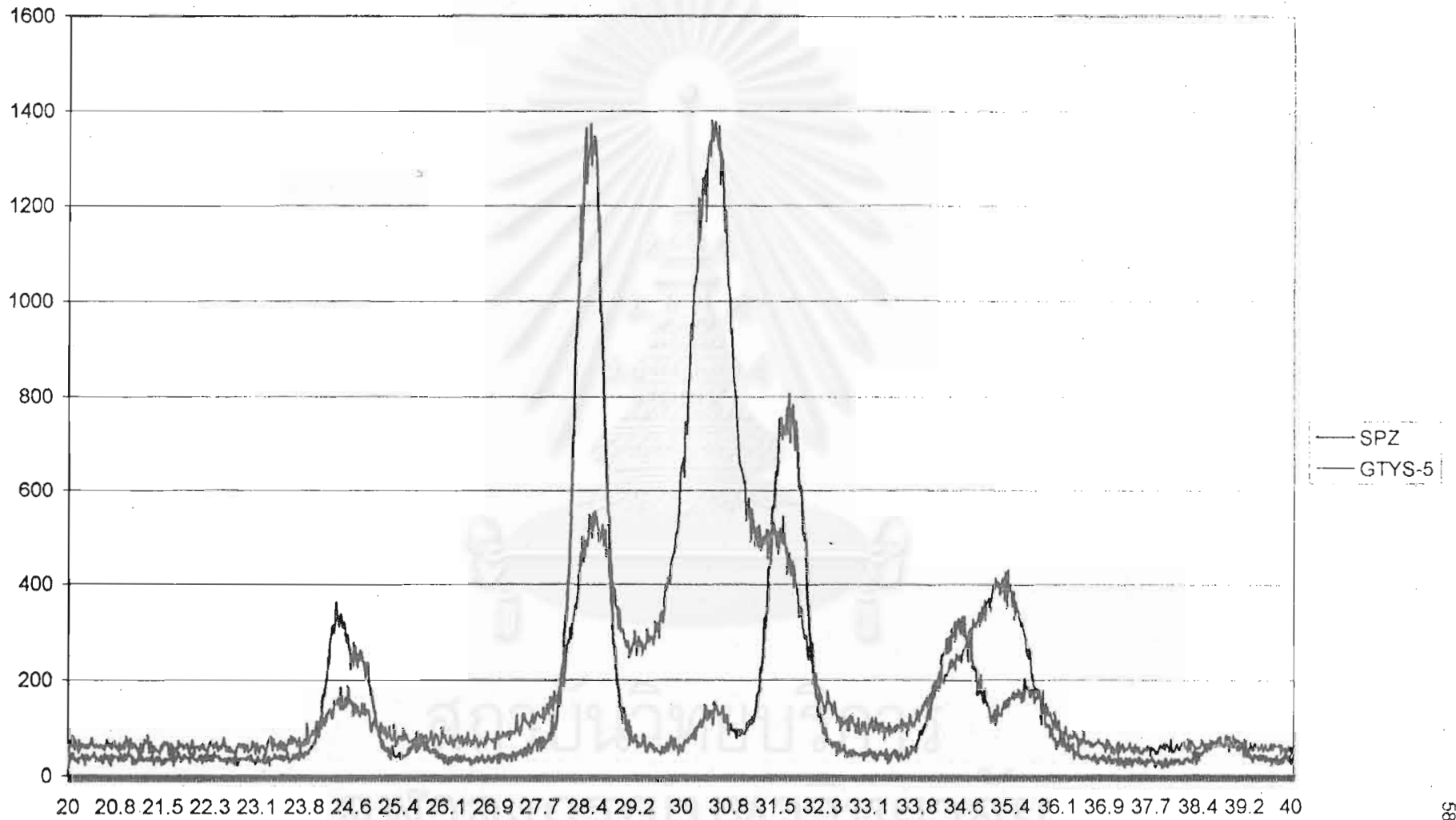
XRD pattern of AM-21 alumina powder



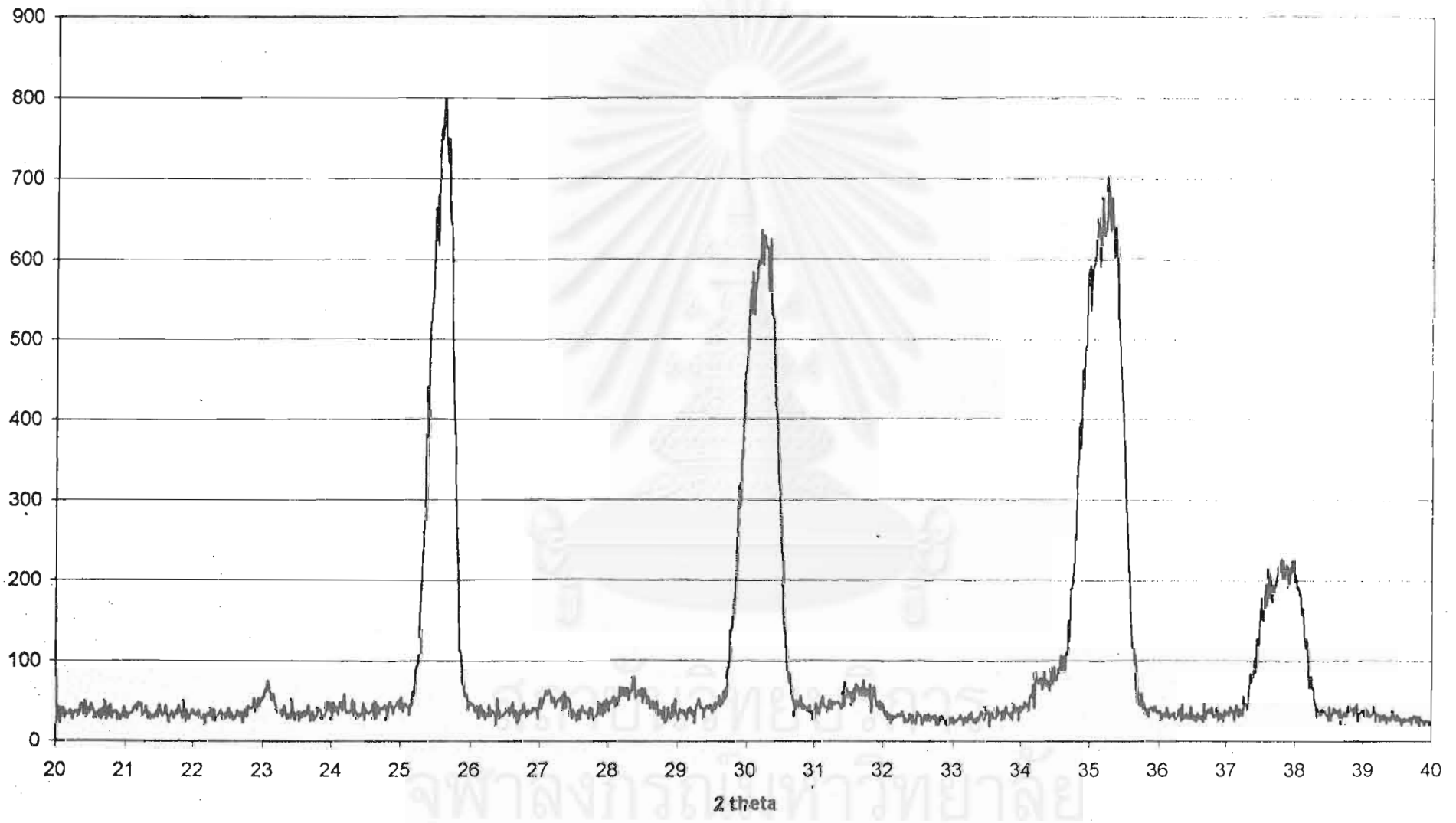
XRD pattern of SPZ zirconia powder



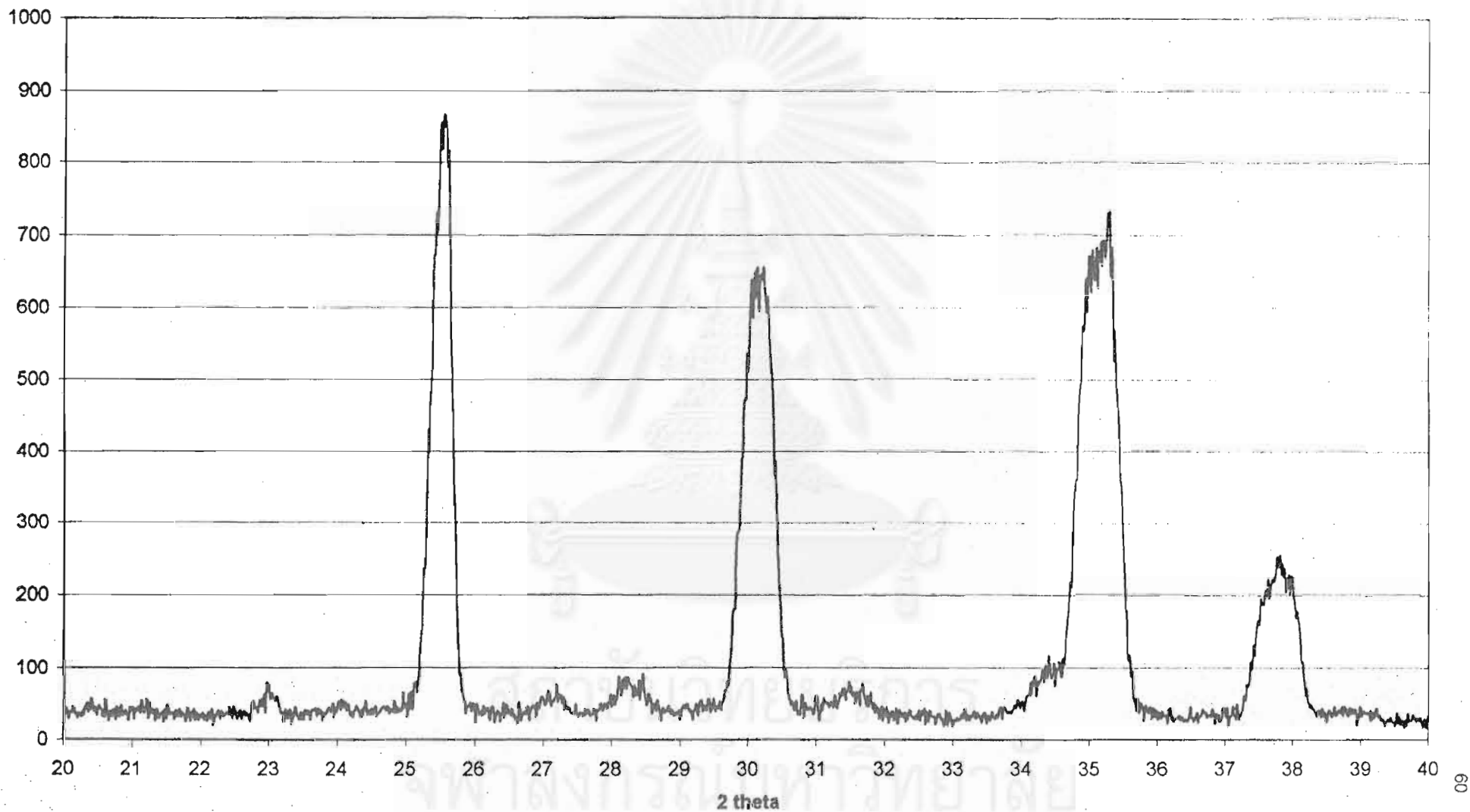
XRD pattern of GTYS-5 zirconia powder



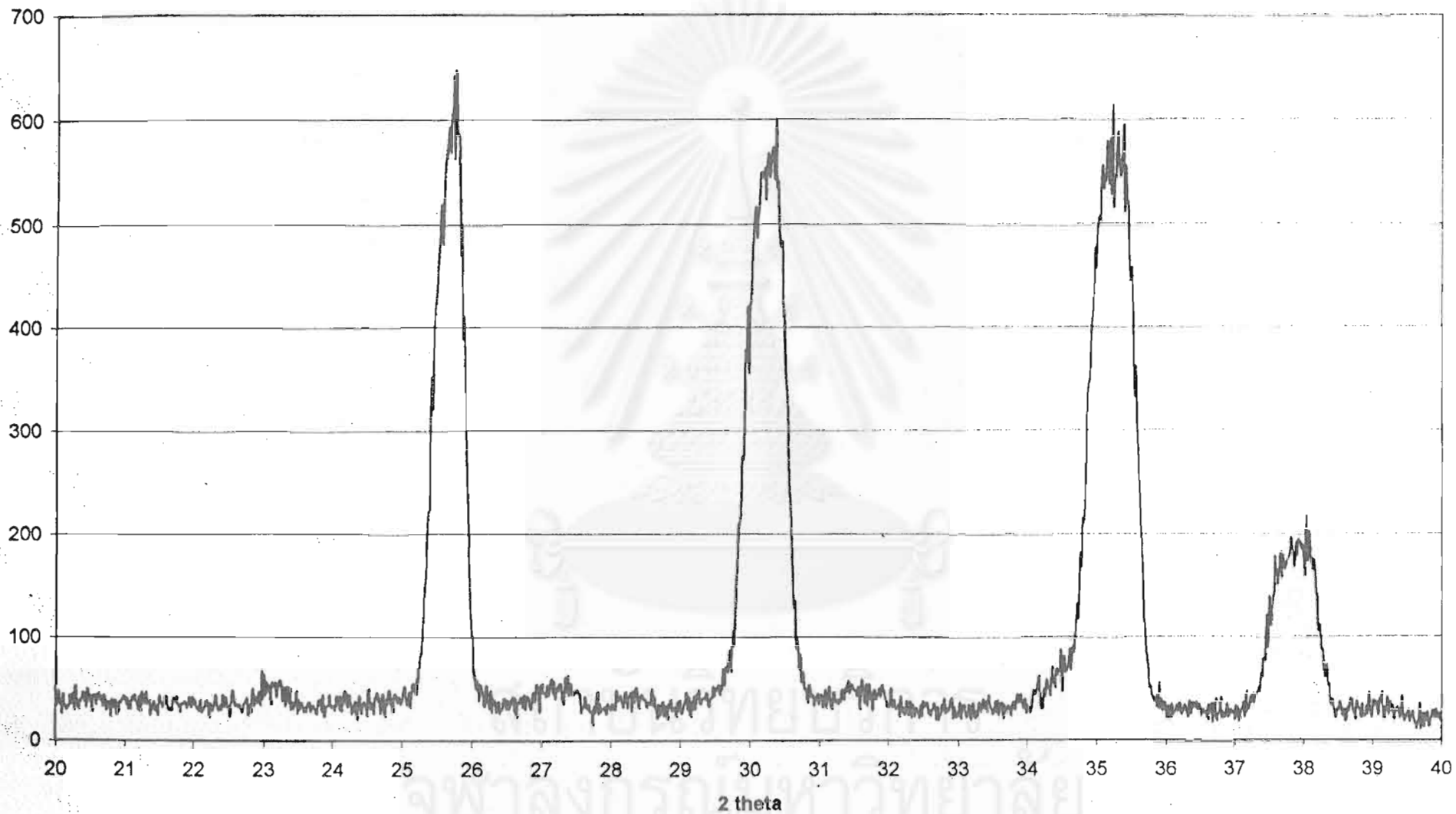
XRD patterns of SPZ and GTYS-5 zirconia powders



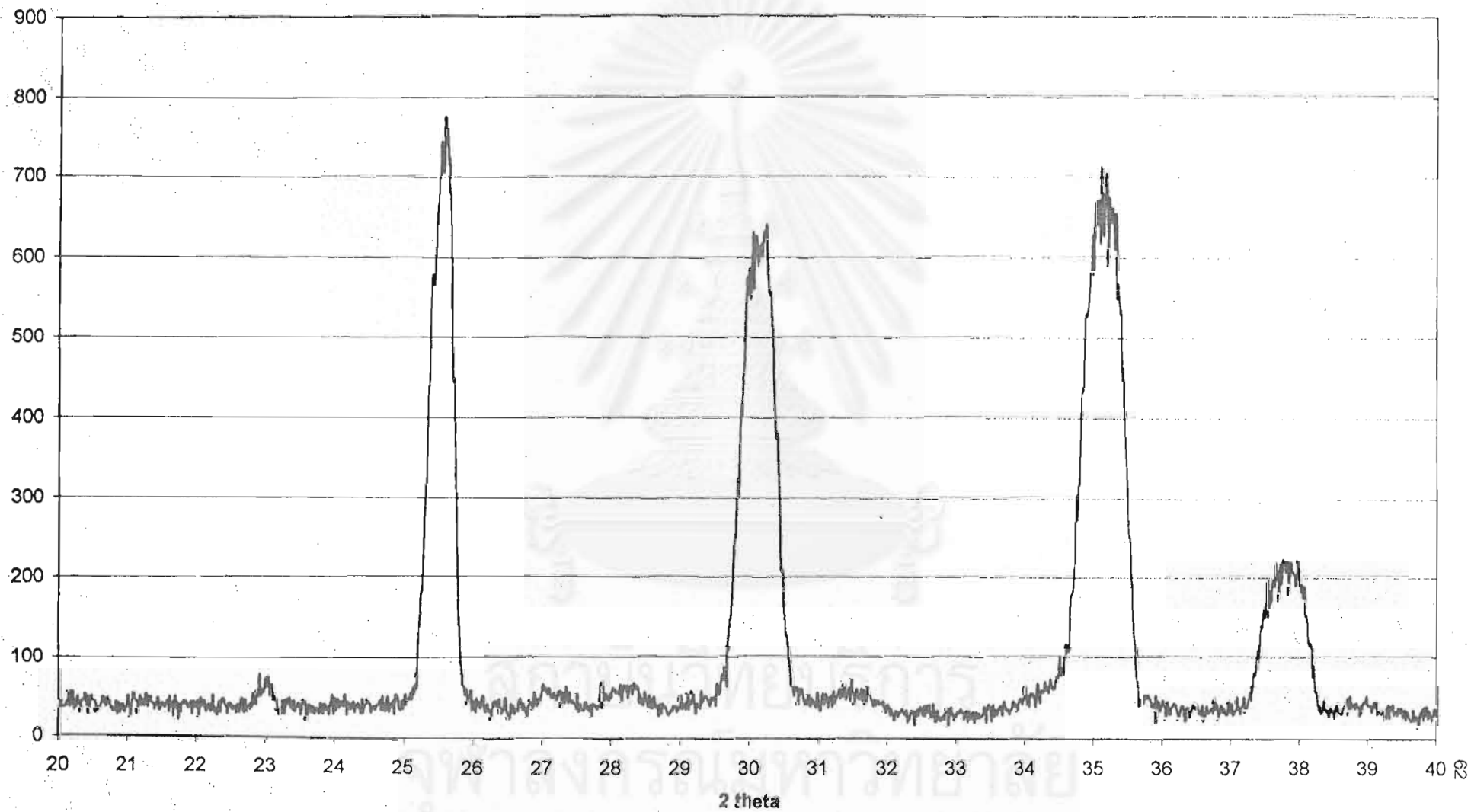
XRD pattern of KM05 sintered at 1600°C



XRD pattern of KM05 sintered at 1650°C



XRD pattern of KM 08 sintered at 1600°C



XRD pattern of KM08 sintered at 1650°C

Biography

Mr. Kamol Panmaung was born on the 23th of March 1980, in Bangkok. After graduated with a Bachelor's Degree in Ceramics and Materials Science from Faculty of Science, Chulalongkorn University in 2000, he enrolled in Master's Degree course in Ceramic Technology, Faculty of Science, Chulalongkorn University in 2001 and graduated in June 2004.



สถาบันวิทยบริการ
จุฬาลงกรณ์มหาวิทยาลัย